Inorganic Chemistry

ARTICLE

pubs.acs.org/IC

Lanthanide dota-like Complexes Containing a Picolinate Pendant: Structural Entry for the Design of Ln^{III}-Based Luminescent Probes

Martín Regueiro-Figueroa,[†] Bachir Bensenane,[‡,∥] Erika Ruscsák,[§] David Esteban-Gómez,[†] Loïc J. Charbonnière,[‡] Gyula Tircsó,[*,§] Imre Tóth,[§] Andrés de Blas,[†] Teresa Rodríguez-Blas,[†] and Carlos Platas-Iglesias[*,†]

[†]Departamento de Química Fundamental, Universidade da Coruña, Campus da Zapateira-Rúa da Fraga 10, 15008 A Coruña, Spain

[‡]Laboratoire d'Ingénierie Moléculaire Appliquée à l'Analyse, IPHC, UMR 7178 CNRS-UdS, ECPM, 25 rue Becquerel, 67087 Strasbourg Cedex, France

[§]Department of Inorganic and Analytical Chemistry, University of Debrecen, P.O. Box 21, Egyetem tér 1, H-4010, Debrecen, Hungary

[∥]Laboratoire de chimie des matériaux, Faculté des sciences, Université d'Oran, B. P. 1524 El-Menouer, 31000 Oran, Algeria

Supporting Information

ABSTRACT: In this contribution we present two ligands based on a do3a platform containing a picolinate group attached to the fourth nitrogen atom of the cyclen unit, which are designed for stable lanthanide complexation in aqueous solutions. Potentiometric measurements reveal that the thermodynamic stability of the complexes is very high (log K = 21.2−23.5), being comparable to that of the dota analogues. Luminescence lifetime measurements performed on solutions of the Eu^{III} and Tb^{III} complexes indicate that the complexes are nine coordinate with no inner-sphere water molecules. A combination of density functional theory (DFT) calculations and NMR measurements shows that for the complexes of the heaviest lanthanides there is a major isomer in solution consisting of the enantiomeric pair $\Lambda(\delta\delta\delta\delta)$ and $\Delta(\lambda\lambda\lambda\lambda)$, which provides square antiprismatic coordination (SAP) around the metal ion. Analysis of the Yb^{III}-induced paramagnetic shifts unambiguously confirms that these complexes have SAP coordination in aqueous solution. For the light lanthanide ions however both the SAP and twisted-square antiprismatic (TSAP) isomers are present in solution. Inversion of the cyclen ring appears to be the rate-determining step for the $\Lambda(\delta\delta\delta\delta) \leftrightarrow \Delta(\lambda\lambda\lambda\lambda)$ enantiomerization process observed in the Lu^{III} complexes. The energy barriers obtained from NMR measurements for this dynamic process are in excellent agreement with those predicted by DFT calculations. The energy barriers calculated for the arm-rotation process are considerably lower than those obtained for the ring-inversion path. Kinetic studies show that replacement of an acetate arm of dota by a picolinate pendant results in a 3-fold increase in the formation rate of the corresponding Eu^{III} complexes and a significant increase of the rates of acid-catalyzed dissociation of the complexes. However, these rates are 1−2 orders of magnitude lower than those of do3a analogues, which shows that the complexes reported herein are remarkably inert with respect to metal ion dissociation.

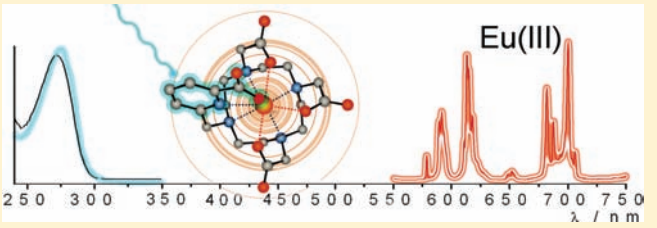

INTRODUCTION

The successful biomedical application of lanthanide chelates both in diagnostics[1] and in therapy[2] has promoted a fast development of lanthanide coordination chemistry in aqueous solution during the last two decades.[3] Furthermore, luminescent lanthanide complexes offer exceptional photophysical properties that find applications in different fields such as biomedical analyses and imaging.[4] A Ln^{III}-based luminescent probe for bioanalytical applications should fulfill a number of requirements: (i) water solubility; (ii) the presence of chromophoric groups suitable for energy transfer to the metal ion of interest (antenna effect);[5] (iii) a high thermodynamic and/or kinetic stability under physiological conditions; (iv) protection of the metal ion from the environment to minimize quenching processes; (v) long excited state lifetimes suitable for time-resolved analysis; (vi) easy functionalization with groups suitable for coupling to biological material.

Macrocyclic derivatives based on 1,4,7,10-tetraazacyclododecane (cyclen) are among the most widely used ligands for stable lanthanide complexation in water. The most important representative of this family of ligands is H_4dota [1,4,7,10-tetraazacyclododecane-1,4,7,10-tetraacetic acid, Chart 1], which forms lanthanide complexes of exceptionally high thermodynamic stability and kinetic inertness.[6] Lanthanide complexes of the heptadentate ligand H_3do3a [1,4,7,10-tetraazacyclododecane-1,4,7-triacetic acid, Chart 1] have been also extensively studied due to their relatively high stability and kinetic inertness to metal

Received: January 27, 2011
Published: April 01, 2011

Chart 1. Ligands Discussed in This Paper

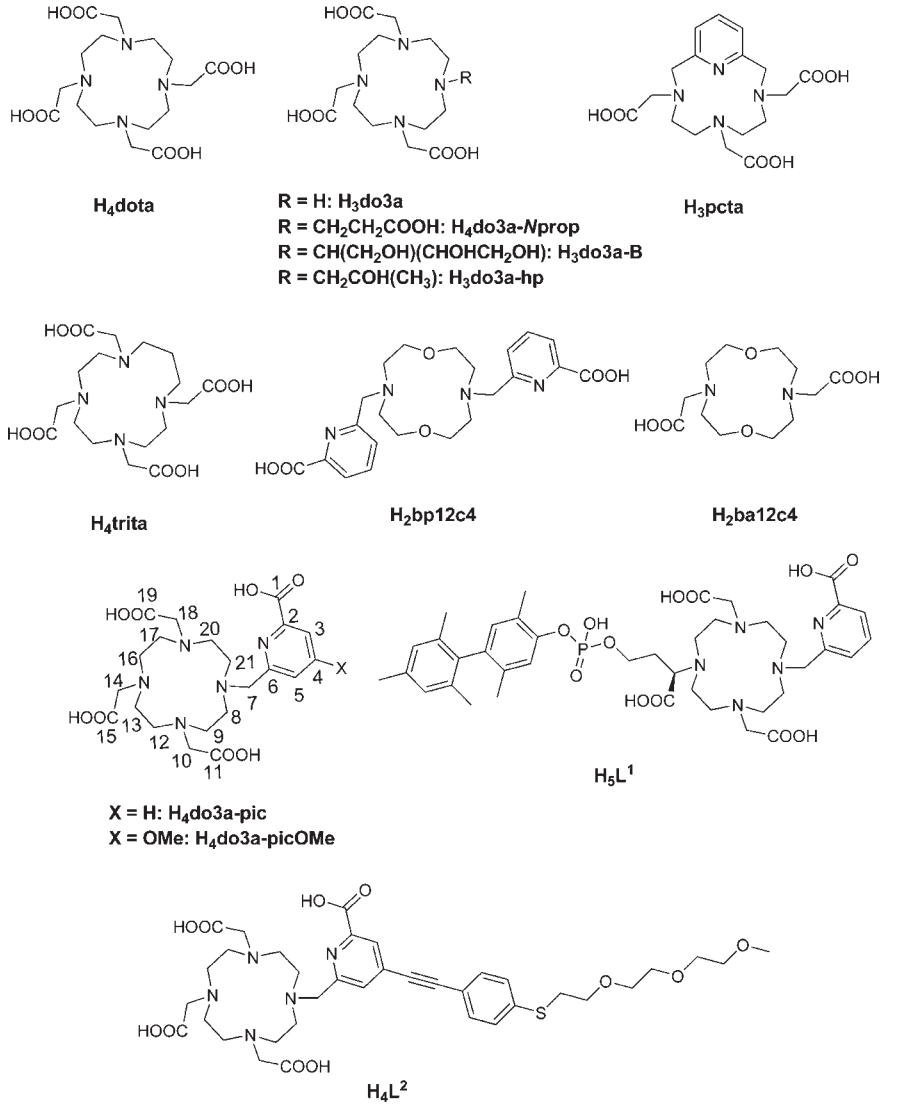

dissociation.[7,8] Furthermore, H_3do3a can be easily functionalized on its secondary amine nitrogen atom, which has led to widespread use of Ln^{III}–do3a derivatives in molecular imaging, generally as unsymmetrical substituted derivatives targeted with biologically,[9] chemically,[10] or photochemically[11] active moieties.

It has been demonstrated that lanthanide complexes of polydentate ligands containing picolinate pendants are of potential interest for application in time-resolved luminescence imaging.[12] Indeed, polydentate ligands containing picolinate moieties anchored on both linear[13] and macrocyclic[14] platforms have been shown to provide remarkably high thermodynamic stability to their Ln^{III} complexes together with a relatively efficient sensitization of ions that emit in the visible region of the spectrum such as Eu^{III} and Tb^{III}. Furthermore, it has been shown that picolinate and dipicolinate moieties may be easily functionalized in the 4-position of the pyridine ring following palladium-catalized coupling reactions[15] and copper(I)-catalyzed azide–alkyne cycloaddition reactions,[16] thereby allowing one to tune the photophysical properties and/or solubility of the corresponding Ln^{III} complexes. These synthetic strategies are also expected to allow functionalization of picolinate units with groups suitable for coupling to biological material.

Zech et al. reported complex $[Gd(L^1)]^{2-}$ (Chart 1), which contains a do3a cage attached to a biphenyl group that confers the system a high affinity for human serum albumin.[17] Pulsed ^{1}H ENDOR spectroscopy demonstrated the absence of inner-sphere water molecules coordinated to the metal ion in this complex. Furthermore, while our work was in progress Maury et al.[18] reported the synthesis and photophysical properties of $Na[Eu(L^2)]$ (Chart 1). This compound was shown to exhibit excellent photophysical properties and a high emission quantum yield. The synthesis of related ligands containing hydroxymethyl or 6-benzylaminocarbonyl groups as a substituent in the 6-position of the pyridyl ring have been reported in the patent literature.[19] However, the coordinative properties of these ligands were not explored further. Herein, we report ligands H_4do3a-pic and H_4do3a-picOMe (Chart 1), which contain a do3a unit functionalized with a picolinate moiety and are expected to provide good protection of the Ln^{III} ions from coordination of water molecules. Ligand H_4do3a-picOMe, which

dx.doi.org/10.1021/ic2001915 |Inorg. Chem. 2011, 50, 4125–4141

Scheme 1. Synthetic Pathway for the Ligands Used in This Work

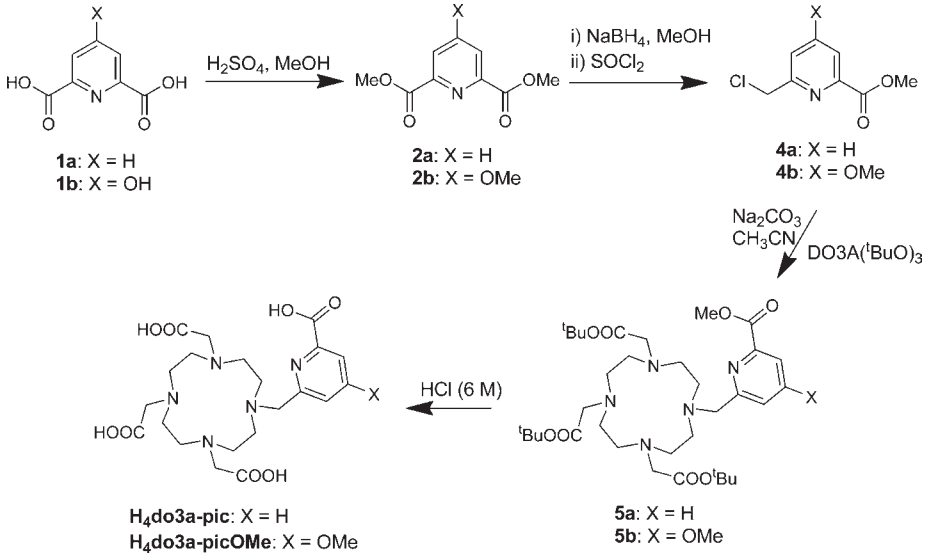

contains a methoxy group in the 4-position of the picolinate unit, was designed as a model for more complicated 4-substituted derivatives with potential application in biomedical analyses. The protonation constants of the ligands as well as the thermodynamic stability constants of different Ln^{III} complexes were determined using pH-potentiometry. The structure and dynamics of the Ln^{III} complexes were investigated by ^{1}H and ^{13}C NMR techniques in D_2O solution. The luminescence properties of the Eu^{III} and Tb^{III} complexes were investigated, allowing one to determine the hydration number of the complexes in solution. In addition, the complexes were characterized by density functional theory (DFT) calculations carried out at the B3LYP level. The structures established by these calculations for the Yb^{III} complexes were compared with the structural information obtained in solution from paramagnetic NMR measurements (Yb^{III}-induced ^{1}H NMR shifts). DFT calculations were also used to investigate the dynamic behavior of these complexes in solution. We also followed the kinetics of formation of the Eu^{III} complex of do3a-pic^{4-} as well as the acid-catalyzed dissociation of the [Ln(do3a-pic)]$^{-}$ complexes (Ln = Ce, Gd, or Yb).

RESULTS AND DISCUSSION

Synthesis and Characterization of the Ligands and Their Ln^{III} Complexes. The synthetic procedure used for preparation of ligands H_4do3a-pic and H_4do3a-picOMe is outlined in Scheme 1. Synthesis of the ligands was achieved in five steps from pyridine-2,6-dicarboxylic acid (**1a**) or 4-hydroxypyridine-2,6-dicarboxylic acid (**1b**). Compounds **2a,b** were prepared via esterification reactions of **1a,b** using H_2SO_4 in methanol. As expected, in the case of **1b** esterification of the carboxylic acid groups was accompanied by introduction of a methoxy substituent on the pyridine 4-position.[20] The 6-chloromethylpyridine derivatives **4a** and **4b** were prepared in good yield by partial reduction of the methyl esters **2a,b** followed by reaction of the intermediate alcohol with $SOCl_2$. *N*-Alkylation of do3a(*t*-BuO)$_3$[21] with **4a,b** in refluxing acetonitrile in the presence of Na_2CO_3 gave compounds **5a,b** in good yields (>80%). Full deprotection of the methyl and *tert*-butyl esters of **5a,b** was cleanly achieved with 6 M HCl to give the desired ligands with overall yields of 41% (H_4do3a-pic) and 42% (H_4do3a-picOMe) as calculated from **1a** and **1b**, respectively. Reaction of ligands H_4do3a-pic or H_4do3a-picOMe with lanthanide triflates in the presence of an excess of triethylamine resulted in formation of compounds of formula (Et_3NH)[Ln(L)] (L = do3a-pic or do3a-picOMe; Ln = La, Eu, Gd, Tb, Yb, or Lu), which were isolated in 70−84% yields. The high-resolution mass spectra (ESI-MS) show peaks due to the [Ln(L)]$^{-}$ entities, thereby confirming formation of the desired compounds.

Ligand Protonation Constants and Stability Constants of the Ln^{III} Complexes. The protonation constants of do3a-pic^{4-} as well as the stability constants of its metal complexes formed with selected Ln^{III} ions were determined by pH-potentiometric titrations; the constants and standard deviations are given in Table 1, which also lists the protonation constants and stability constants of Ln^{III} complexes formed with related ligands (Chart 1). Owing to the relatively slow rates of complexation often involving Ln^{III} ions and macrocyclic ligands, the stability constants were determined with the use of the out-of-cell technique. The ligand protonation constants are defined as in eq 1, and the stability constants of the metal chelates and the protonation constants of the complexes are expressed in eqs 2 and 3, respectively.

$$K_i^{H} = \frac{[H_iL]}{[H_{i-1}L][H^+]} \quad (1)$$

$$K_{ML} = \frac{[ML]}{[M][L]} \quad (2)$$

$$K_{MHL} = \frac{[MHL]}{[ML][H^+]} \quad (3)$$

The data compared in Table 1 indicate that the first protonation constant is lower in do3a-pic^{4-} than in dota as a consequence of the electron-withdrawing effect of the picolinate pendant arm.[28] Similar effects can be observed when the protonation constants

dx.doi.org/10.1021/ic2001915 |*Inorg. Chem.* 2011, 50, 4125–4141

Table 1. Protonation Constants of do3a-pic^{4-} and Related Ligands and Stability Constants of their Ln^{III} Complexes (25 °C)[a]

	do3a-pic^{4-}	dota^{4-}	ba12c4^{2-h}	bp12c4^{2-i}	do3a^{3-}
log K_1^H	10.91(1);[b] 9.21(2)[c]	12.09;[d] 12.6[e]	9.53	9.16	11.59;[j] 11.55[k]
log K_2^H	9.41(2);[b] 8.94(1)[c]	9.67;[d] 9.70[e]	7.46	7.54	9.24;[j] 9.15[k]
log K_3^H	4.89(3);[b] 4.82(2)[c]	4.55;[d] 4.50[e]	2.11	3.76	4.43;[j] 4.48[k]
log K_4^H	3.79(3);[b] 3.52(2)[c]	4.09;[d] 4.14[e]		2.79	3.48[j]
log K_5^H	1.72(3);[b] 1.39(2)[c]	2.32[e]			
Σlog K_i^H	30.73;[b] 27.88[c]	30.40;[d] 33.26[e]	19.1	23.25	28.74[j]
log K_{LaL}	21.17(4)	22.86[f]		16.81	
log K_{LaHL}	2.55(9)				
log K_{CeL}					19.7[k]
log K_{EuL}	23.46(2)	23.45[f]		18.62	20.69[l]
log K_{EuHL}	2.72(2)				
log K_{GdL}	23.31(4)	24.67;[f] 25.3[g]		18.82	21.1;[k] 22.02[m]
log K_{GdHL}	2.65(4)				2.06[k]
log K_{YbL}				18.08	
log K_{LuL}	22.82(5)	25.41[f]			23.0[k]
log K_{LuHL}	2.48(6)				

[a] Standard deviations are shown in parentheses; ΔV = 0.0019, 0.00054, 0.0012, and 0.0016 cm^3 for the La, Eu, Gd, and Lu systems, respectively. [b] I = 0.1 M KCl. [c] I = 0.15 M NaCl. [d] I = 0.1 M KCl, ref 22. [e] I = 1.0 M Me_4NCl, ref 23. [f] Reference 24. [g] Reference 7a. [h] I = 0.1 M KCl, ref 25. [i] I = 0.1 M KCl, ref 14c. [j] I = 0.1 M Me_4NCl, ref 7a. [k] I = 0.1 M KCl, ref 7a. [l] Reference 26. [m] I = 0.1 M Me_4NCl, ref 27.

of H_2ba12c4 and H_2bp12c4 ligands (or the analogues derived from 15-crown-5[29] and 18-crown-6[30]) are compared, although in these cases the decreases are less pronounced. The decrease is even more important when 0.15 M NaCl is used as an ionic background. This finding indicates that the do3a-pic^{4-} ligand forms noticeably stable complexes with the Na^+ ions. The stability constant of the [Na(do3a-pic)] complex was also calculated from the titration curve obtained in 0.15 NaCl. The value obtained in this medium is slightly lower than that of [Na(dota)] (log K_{NaL} − log K_{KL} = 3.73 and 4.23 for do3a-pic^{4-} and dota^{4-} ligands, respectively). This is most likely a consequence of the lower overall basicity of do3a-pic^{4-} in comparison to dota (approximately 3 log K units).[31]

Data from the batch samples prepared for the Ln^{III} ions were fitted to an equilibrium model in which formation of parent complexes with a 1:1 metal to ligand ratio (Ln:do3a-pic) was assumed. However, the standard deviation values significantly decreased when formation of protonated complexes [Ln(Hdo3a-pic)] was also taken into account, which indicates that protonated complexes are presumably formed under these conditions. The log K_{LnL} values of the [Ln(do3a-pic)]$^-$ complexes along with data available in the literature for complexes of structurally related ligands are listed in Table 1. Since the stability data for the Ln^{III} complexes of ba12c4^{2-} are not available in the literature, the data of some [Ln(do3a)] complexes are shown for comparative proposes.

The data presented in Table 1 show that the stability of Ln^{III} complexes of do3a-pic^{4-} increases from the early lanthanides to the middle of the series and then remains relatively constant with a slight decrease for the heaviest lanthanides. In this respect, this chelator is similar to bp12c4^{2-}, in contrast to most of the macrocyclic poly(amino carboxylate) ligands, such as dota^{4-} or do3a^{3-}, and the most important open chain complexometric reagent, edta^{4-}, which form complexes of increasing stability all across the lanthanide series because of the increase of charge density on the metal ions. This suggests that the presence of a relatively bulky picolinate unit in do3a-pic^{4-} causes some steric

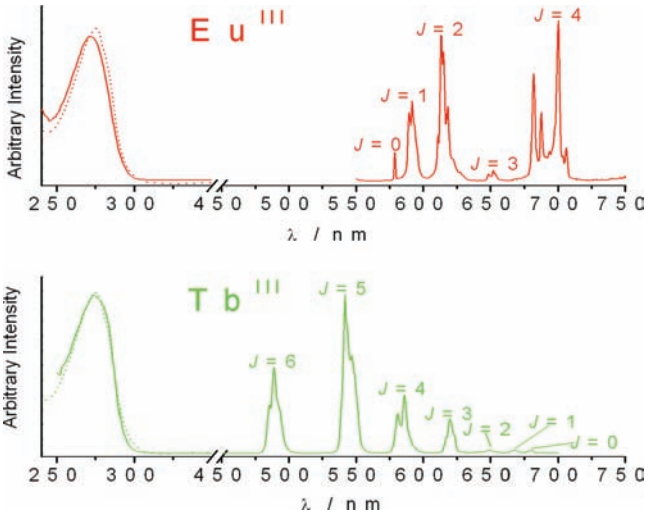

Figure 1. Absorption (dotted lines), excitation, and emission spectra of [Ln(do3a-pic)]$^-$ complexes (Ln = Eu or Tb) as recorded in 2.0 × 10^{-4} M aqueous solutions (TRIS buffer, pH = 7.0).

hindrance for coordination of the ligand to the smaller Ln^{III} ions. For the first half of the lanthanide series (La−Gd), the log K_{ML} values determined for do3a-pic^{4-} complexes show that their stability is only slightly lower than that reported for the dota analogues and 1.5−3.4 log K units higher than that of do3a^{3-} derivatives. However, due to the smooth decrease of the stability constants of do3a-pic^{4-} complexes along the second half of the series, the stability of the Lu^{III} complex of do3a-pic^{4-} is somewhat lower than that of the dota^{4-} analogue and very similar to that of the do3a^{3-} complex.

Photophysical Properties. The UV−vis absorption spectra of the Eu^{III} and Tb^{III} complexes of do3a-pic^{4-} and do3a-picOMe^{4-} are displayed in Figure 1 and Figure S1, Supporting Information. The relevant spectroscopic data are also presented

dx.doi.org/10.1021/ic2001915 |Inorg. Chem. 2011, 50, 4125–4141

Table 2. Spectroscopic Properties of the Complexes of do3a-pic^{4-} and do3a-picOMe^{4-} in Aqueous Solutions

		Eu		Tb	
		do3a-pic	do3a-picOMe	do3a-pic	do3a-picOMe
absorption	λ_{max}/nm (ε/M$^{-1}\cdot$cm^{-1})	275 (3050)	271 (2500)	275 (3540)	276 (1600)
			242 (4390)		242 (3740)
emission	Φ_{TRIS}/%	24	9	56	58
	τ_{TRIS}/ms	1.20	1.10	3.22	3.00
	τ_{H2O}/ms	1.06	1.13	2.90	2.89
	τ_{D2O}/ms	2.15	2.08	3.49	3.74
	q^a	0.2	0.1	0.1	0.2
	η_{sens}/%^{a}	quant.	45		
	τ_R/ms^a	5.28	5.36		
	Φ_{Eu}/%^{a}	23	21		

[a] See Experimental Section and text for the details of the calculations.

in Table 2. The UV−vis absorption spectra of the complexes of do3a-pic^{4-} display a broad absorption band with maximum at 275 nm corresponding to $\pi \rightarrow \pi^*$ transitions centered on the pyridyl carboxylate moieties.[32] Introduction of the methoxy group in the para position of the pyridyl ring resulted in a drastic change of the absorption spectra with a very strong absorption band appearing on the high-energy tail of the spectra (Figure S1, Supporting Information). Introduction of the electron-donating moiety probably resulted in a more important contribution of n $\rightarrow \pi^*$ transitions to the overall band envelope, the final spectrum displaying two shoulders at ca. 242 and 276 nm.

Upon excitation into the UV absorption bands of the complexes, the emission spectra displayed emission patterns characteristic of the particular lanthanide ion.[33] As an example, Figure 1 displays the emission spectra of [Ln(do3a-pic)]$^-$ complexes (Ln = Eu or Tb) in TRIS buffer at pH = 7.0. As expected, the emission spectrum of the Eu^{III} complex is composed of five regions corresponding to the $^5D_0 \rightarrow {}^7F_J$ transitions at 578 (J = 0), 585−603 (J = 1), 604−637 (J = 2), 646−658 (J = 3), and 673−712 nm (J = 4). By monitoring the emission at 615 nm, the excitation spectrum of the complex perfectly fits with its absorption spectrum, thereby evidencing the antenna effect due to the energy transfer from the ligand to the lanthanide cation.[34] It is to be noticed that the shapes of the emission spectra of both Eu complexes are very similar, pointing to almost identical coordination environments. Similarly, the emission spectra of the Tb complexes (Figure 1) are composed of the characteristic $^5D_4 \rightarrow {}^7F_J$ transitions with maxima at 489 (J = 6), 542 (J = 5), 586 (J = 4), and 620 nm (J = 3). Weaker emission bands corresponding to the J = 2−0 transitions can also be observed around 652, 669, and 681 nm.

The measured luminescence lifetimes for both Eu^{III} and Tb^{III} complexes can be perfectly fitted with monoexponential decays, in agreement with the presence of single-emitting species in solution. Whatever the solvent (H_2O, D_2O, TRIS buffer) the measured lifetimes are very long, as a result of an excellent shielding of the Ln^{III} cations from surrounding water molecules. Using the methodology developed by Horrocks and other groups[35] it was possible to estimate the hydration numbers from the luminescence lifetimes measured in water and heavy water (for details see Experimental Section). The data unambiguously pointed to a hydration number of almost zero, within experimental error, for all complexes. This is in perfect agreement with a coordination sphere saturated by the 9 heteroatoms of the ligand (4 N atoms from the cyclen structure, 4 O atoms from the carboxylate functions, and the N atom of the pyridine ring), as observed for a similar ligand structure in which the carboxypyridine moiety was replaced by a phenantroline one.[36]

The overall luminescence quantum yields of the Tb^{III} complexes are very good, and they remain nearly unaltered by the presence of the methoxy substituent. In contrast, the methoxy functionalization had a very large impact on the luminescence quantum yield of the europium complexes, which dropped from 24% for [Eu(do3a-pic)]$^-$ to 9% for [Eu(do3a-picOMe)]$^-$.

Following the relationships developed by Werts et al.,[37] it was possible to calculate the metal-centered luminescence quantum yield of the europium complexes, Φ_{Eu}, from their emission spectra. According to this treatment, the radiative lifetime of europium, τ_R, can be calculated with eq 4 in which I_{tot} and I_{MD} are, respectively, the total area of the corrected emission spectrum and the area of the magnetic dipole-allowed $^5D_0 \rightarrow {}^7F_1$ transition, n is the refractive index of the medium, and $A_{MD,0}$ is the spontaneous emission probability of this last transition, theoretically calculated to be 14.65 s^{-1}.

$$1/\tau_R = A_{MD,0} n^3 (I_{tot}/I_{MD}) \quad (4)$$

Values of τ_R of 5.28 and 5.36 ms were, respectively, obtained for [Eu(do3a-pic)]$^-$ and [Eu(do3a-picOMe)]$^-$, which are in good agreement with other values reported in the literature for water-soluble Eu^{III} complexes.[37,38] Knowing τ_R, Φ_{Eu} can be calculated using eq 5, leading to 23% and 21% for [Eu(do3a-pic)]$^-$ and [Eu(do3a-picOMe)]$^-$, respectively. Noteworthy, values of both τ_R and Φ_{Eu} are very close for both complexes, reflecting the similar coordination environment of Eu^{III} in both systems. Finally, the sensitization efficiency, η_{sens}, corresponding to the ability of the ligand to transfer energy to the europium cation can be obtained using eq 6

$$\Phi_{Eu} = \tau_{obs}/\tau_R \quad (5)$$

$$\Phi_{ov} = \Phi_{Eu} \times \eta_{sens} \quad (6)$$

where τ_{obs} is the measured luminescence lifetime and Φ_{ov} is the overall luminescence quantum yield, both obtained from the spectroscopic measurements described above. For [Eu(do3a-pic)]$^-$, the sensitization efficiency was found to be quantitative, within experimental uncertainty, and the overall luminescence is governed by the metal-centered luminescence efficiency. In

dx.doi.org/10.1021/ic2001915 |Inorg. Chem. 2011, 50, 4125–4141

contrast, introduction of the methoxy group resulted in a dramatic drop of the sensitization efficiency. This phenomenon was already observed in the case of the europium complexes of 2,6-dipicolinic acid.[39]

Structure and Dynamics of the Complexes in Solution. The ^{1}H and ^{13}C NMR spectra of the diamagnetic La^{III} and Lu^{III} complexes of do3a-pic^{4-} and do3a-picOMe^{4-} were obtained in D_2O solution at pD = 7.0. In the case of the La^{III} analogues the ^{1}H NMR spectra recorded at room temperature show relatively broad signals due to exchange phenomena (Figure S2, Supporting Information). Decreasing the temperature to 278 K did not result in better resolved spectra, which prevented a detailed assignment of the proton signals. By contrast, in the case of the Lu^{III} complexes the ^{1}H spectra are well resolved at 298 K (Figure S3, Supporting Information), while the proton signals broaden only at higher temperatures (see below). The proton spectra of both Lu^{III} complexes consist of 27 signals, which points to a C_1 symmetry of the complexes in solution. Both the ^{1}H and the ^{13}C NMR spectra of Lu^{III} complexes indicate the presence of a single major species in solution. In the case of the La^{III} analogues the ^{1}H NMR spectra recorded in CD_3OD solution at 298 K show two sets of signals for the aromatic protons with a ca. 2:1 intensity ratio, which indicates the presence of two complex species in solution.

The assignments of the proton and carbon signals of the Lu^{III} complexes (Table S1, Supporting Information) were based upon heteronuclear HSQC and HMBC experiments as well as 2D homonuclear COSY, NOESY, and EXSY experiments. The signals due to the CH_2 protons of the acetate pendant arms (H10, H14, and H18, see Chart 1) show AB spin patterns, which indicate a slow interconversion between the Δ and the Λ optical isomers arising from the different orientation of the pendant arms (see below). One of these AB spin patterns is observed at particularly high field (2.86 and 1.97 for [Lu(do3a-pic)]$^-$ and 2.89 and 2.09 for [Lu(do3a-picOMe)]$^-$). Inspection of the DFT-optimized structures described below shows that protons H18 are directed toward the aromatic ring current of the pyridyl ring of the neighbor pendant arm. On this basis, this AB spin system was assigned to protons H18, as the ring current shift effect provoked by the pyridyl unit is expected to cause a shielding of any nuclei above or below that ring.[40]

It is known from previous ^{1}H NMR studies on Ln^{III} complexes with macrocyclic ligands that the ring axial protons experience strong coupling with the geminal protons and the vicinal axial protons while the equatorial protons provide strong coupling with the geminal protons only.[41] Indeed, the $^3J_{H-H}$ coupling constants characterizing the coupling between vicinal pairs of protons (axial−axial, axial−equatorial, and equatorial−equatorial) follow the Karplus equation [$^3J_{H-H} = 7 - \cos\phi + 5\cos 2\phi$, where ϕ represents the H−C−C−H dihedral angle and $^3J_{H-H}$ is given in Hertz].[42] According to our DFT calculations (see below), the ϕ values involving axial−axial vicinal protons are close to 180° (175.8−179.1°) while the dihedral angles defined by axial−equatorial and equatorial−equatorial vicinal protons fall within the range 52.2−63.3°. Thus, the specific assignment of the axial and equatorial protons could be achieved by observing the cross-peaks in the COSY spectra, as axial protons are expected to give two strong (geminal and axial−axial) and one weak (axial−equatorial) cross-peaks, whereas equatorial protons should show one strong (geminal) and two weak (equatorial−equatorial and equatorial−axial) cross-peaks. The signals due to ring axial proton nuclei positioned above the plane defined by the four amine nitrogen atoms (H8ax, H12ax, H16ax, and H20ax) are observed at considerably higher fields than those of ring axial proton nuclei placed below that plane (H9ax, H13ax, H17ax, and H21ax). This is attributed to the diamagnetic shielding effect on the chemical shifts of protons that lie below the plane of the neighboring carbonyl (H8ax, H12ax, or H16ax) or pyridyl (H20ax) groups (Chart 2).[40]

Chart 2. Schematic Representation of the Conformation Adopted by the [Lu(do3a-pic)]$^-$ and [Lu(do3a-picOMe)]$^-$ Complexes Showing the Shielding Effect of the Aromatic Ring Current of the Picolinate Moiety on the H20ax Proton

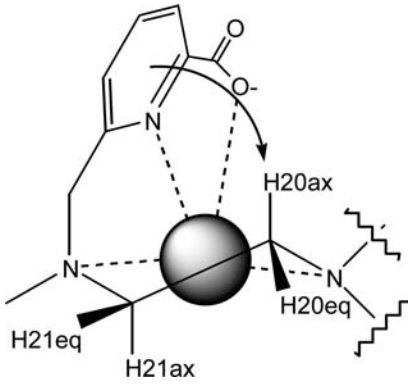

Luminescence lifetime measurements indicate that the Eu^{III} and Tb^{III} complexes of do3a-pic^{4-} and do3a-picOMe^{4-} do not contain inner-sphere water molecules (see above). Thus, to obtain information on the solution structure of the Ln^{III} complexes of these ligands we characterized the [Ln(do3a-pic)]$^-$ and [Ln(do3a-picOMe)]$^-$ (Ln = La, Gd, Yb, or Lu) systems by means of DFT calculations (B3LYP model, see Computational Methods). In our calculations solvent effects (water) were taken into account using the polarizable continuum model (PCM).

It is well known that in nine-coordinate Ln^{III} dota-like complexes the four ethylenediamine groups adopt gauche conformations giving rise to two macrocyclic ring conformations: ($\delta\delta\delta\delta$) and ($\lambda\lambda\lambda\lambda$). Furthermore, there are two possible orientations of the four pendant arms (absolute configuration Δ or Λ) resulting in four possible steroisomers, existing as two enantiomeric pairs.[43] These stereoisomers differ by the layout of the four acetate arms, adopting either a monocapped square-antiprismatic (SAP) or a monocapped twisted square-antiprismatic (TSAP) geometry.[44] Our calculations performed on the [Ln(do3a-pic)]$^-$ and [Ln(do3a-picOMe)]$^-$ systems provide the SAP and TSAP isomers as minimum energy conformations (Figure S4, Supporting Information). The coordination polyhedron around the lanthanide ion may be considered to be comprised of two virtually parallel pseudo-planes: the four amine nitrogen atoms define the lower plane (P_{N4}), while the three oxygen atoms of the acetate groups coordinated to the metal ion and the nitrogen atom of the pyridine unit define the upper plane (P_{NO3}). The oxygen atom of the picolinate moiety involved in coordination to the Ln^{III} ion is capping the upper plane. Calculated bond distances of the metal coordination environments are listed in Table S2 (Supporting Information). The distances between the metal ions and the donor atoms of the ligand decrease along the lanthanide series, as usually observed for Ln^{III} complexes as a consequence of the lanthanide contraction.[45] The average Ln−O distances obtained from

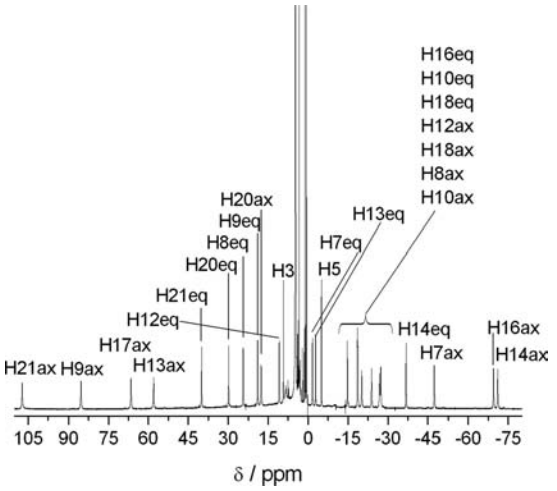

Figure 2. ^{1}H NMR spectrum (300 MHz) of $[Yb(do3a\text{-}picOMe)]^-$ recorded in D_2O solution at 298 K.

DFT calculations are in excellent agreement with those observed in the solid state for Ln^{III} dota-like complexes.[46] The mean twist angles ω[47] between the two parallel squares range from ca. 32° to 36° and −19° to −22° for the SAP and TSAP isomers, respectively. These values are very similar to those observed in the solid state for the respective isomers of dota complexes.[48]

The binding of a ligand to a paramagnetic Ln^{III} ion generally results in large NMR frequency shifts at the ligand nuclei, with magnitudes and signs depending on both the nature of the lanthanide ion and the location of the nucleus relative to the metal center.[49] For a given nucleus i, the isotropic paramagnetic shift induced by a lanthanide ion j (δ_{ij}^{para}) is generally a combination of the Fermi contact (δ_{ij}^{con}) and dipolar (δ_{ij}^{dip}) contributions[49]

$$\delta_{ij}^{para} = \delta_{ij}^{exp} - \delta_i^{dia} = \delta_{ij}^{con} + \delta_{ij}^{dip} \quad (7)$$

where the diamagnetic contribution δ_i^{dia} is obtained by measuring the chemical shifts for analogous diamagnetic complexes (the Lu^{III} complexes in the present case). The hyperfine ^{1}H NMR shifts in Yb^{III} complexes are considered to be largely pseudocontact in origin,[50] and we therefore initiated the analysis of the paramagnetic shifts observed in the ^{1}H NMR spectra of the Yb^{III} complexes of do3a-pic^{4-} and do3a-picOMe^{4-} with the assumption that they are dominated by dipolar contributions, as given by the following equation

$$\delta_{ij}^{dip} = D_1\frac{3\cos^2\theta - 1}{r^3} + D_2\frac{\sin^2\theta\cos 2\varphi}{r^3} \quad (8)$$

where r, θ, and φ are the spherical coordinates of the observed nucleus with respect to Ln^{III} at the origin and D_1 and D_2 are proportional, respectively, to the axial $[\chi_{zz} - 1/3(\chi_{xx} + \chi_{yy} + \chi_{zz})]$ and rhombic $(\chi_{xx} - \chi_{yy})$ anisotropies of the magnetic susceptibility tensor χ. In the special case of axial symmetry the second term of eq 8 vanishes since $D_2 = 0$.

The ^{1}H NMR spectra of the $[Yb(do3a\text{-}pic)]^-$ and $[Yb(do3a\text{-}picOMe)]^-$ complexes recorded in D_2O solution are well resolved (Figure 2). They consist of 27 signals, which points to a C_1 symmetry of the complexes in solution. The assignments of the proton signals (Table 3) were based on standard 2D homonuclear COSY experiments, which gave strong cross-peaks between the geminal CH_2 protons as well as between vicinal axial−axial protons of the cyclen unit. A full assignment of the proton spectra was achieved with the SHIFT ANALYSIS program developed by Forsberg,[51] which allows one to perform random permutations of the observed dipolar shifts.

The SAP and TSAP geometries of $[Yb(do3a\text{-}pic)]^-$ and $[Yb(do3a\text{-}picOMe)]^-$ complexes obtained from DFT calculations were used to assess the agreement between the experimental and the predicted Yb^{III}-induced paramagnetic shifts with the SHIFT ANALYSIS program.[51] The SHIFT ANALYSIS program calculates the dipolar shifts defined by eq 8 in the molecular coordinate system using a linear least-squares search

Table 3. ^{1}H Shifts (ppm with respect to TMS) for the Yb^{III} Complexes of do3a-pic^{4-} and do3a-picOMe^{4-}, and Comparison of Experimental (δ_i^{para}) and Calculated (δ_i^{dip}) Paramagnetic ^{1}H Shifts (ppm)

	do3a-pic^{4-}			do3a-picOMe^{4-}		
	δ_i^{exp}	δ_i^{para}[a]	δ_i^{dip}[b]	δ_i^{exp}	δ_i^{para}[a]	δ_i^{dip}[b]
H3	11.84	−3.90	−3.08	9.27	−1.83	−0.37
H4	3.52	4.61	4.05			
H5	−1.01	8.65	6.78	−5.11	12.23	10.23
H7ax	−44.47	48.67	45.62	−47.43	51.50	49.10
H7eq	0.71	3.42	−0.59	−1.68	5.75	1.66
H8ax	−33.54	36.14	31.39	−26.90	29.85	24.33
H8eq	20.07	−17.47	−19.65	24.38	−21.43	−23.98
H9ax	78.75	−75.22	−74.54	85.45	−81.94	−81.44
H9eq	15.34	−12.36	−15.68	19.01	−16.43	−19.52
H10ax	−23.06	26.39	33.67	−27.38	30.71	37.82
H10eq	−19.85	23.50	21.11	−18.50	22.14	19.69
H12ax	−9.30	12.04	8.56	−20.18	22.91	19.30
H12eq	13.02	−10.16	−12.94	10.93	−8.07	−10.83
H13ax	56.95	−53.52	−50.91	58.17	−54.75	−52.08
H13eq	1.12	1.35	−1.85	−2.74	5.19	1.96
H14ax	−67.39	70.65	82.23	−71.06	74.31	85.73
H14eq	−30.49	34.07	31.23	−36.72	40.30	37.18
H16ax	−71.59	74.28	71.65	−69.56	72.24	69.79
H16eq	−14.71	17.40	13.37	−14.76	17.44	13.23
H17ax	61.50	−58.12	−58.62	66.55	−63.17	−64.40
H17eq	2.19	0.13	−3.88	4.77	−2.46	−6.35
H18ax	−19.64	21.61	24.23	−23.85	25.94	28.90
H18eq	−19.85	22.71	19.52	−18.70	21.59	18.61
H20ax	22.03	−19.64	−24.38	17.53	−14.87	−20.25
H20eq	28.67	−26.04	−28.53	29.82	−27.16	−29.89
H21ax	99.66	−96.09	−88.02	107.30	−103.75	−95.12
H21eq	38.07	−35.38	−36.54	40.00	−37.55	−38.33
−OMe				0.50	3.45	2.34
D_1[c]			−2747			−2972
D_2[c]			−1955			−1589
AF_j[d]			0.1042			0.1012

[a] Positive values correspond to shifts to higher fields. The diamagnetic contribution was estimated from the shifts observed for the Lu^{III} analogue. [b] Values calculated by using eq 8 and the SAP conformations of the complexes optimized in aqueous solution at the B3LYP/6-31G(d) level. [c] In ppm·Å^{-3}. [d] $AF_j = [\Sigma_i(\delta_{ij}^{exp} - \delta_{ij}^{cal})^2/\Sigma_i(\delta_{ij}^{exp})^2]^{1/2}$, where δ_{ij}^{exp} and δ_{ij}^{calc} are represent the experimental and calculated values of a nucleus i in a given Ln^{III} complex j, respectively.

dx.doi.org/10.1021/ic2001915 |Inorg. Chem. 2011, 50, 4125–4141

that minimizes the difference between the experimental and the calculated data. The agreement between the experimental and the calculated isotropic shifts obtained using the TSAP isomers were very poor [$AF_j \approx 0.27$]. However, a much better agreement factor between the experimental and the calculated paramagnetic shifts is obtained when the SAP geometries are used [AF_j = 0.1042 and 0.1012 for the do3a-pic^{4-} and do3a-picOMe^{4-} complexes, respectively]. Table 3 shows the D_1 and D_2 values providing the best fit of the experimental shift values as well as a comparison of the experimental and calculated paramagnetic shifts according to the dipolar model. As expected for nonaxial systems, the calculated D_1 and D_2 values define a rhombic magnetic susceptibility tensor.

The excellent agreement observed between the experimental and the calculated Yb^{III}-induced paramagnetic shifts unambiguously proves that these complexes adopt a SAP geometry in aqueous solution. As discussed above, the ^{1}H NMR spectra of the La^{III} analogues point to the presence of two complex species in solution at 298 K. Different NMR studies on Ln^{III} dota-like complexes have shown that the abundance of the SAP isomer is progressively increasing moving to the right across the lanthanide series.[52] Thus, we conclude that the [Ln(do3a-pic)]$^-$ and [Ln(do3a-picOMe)]$^-$ complexes adopt a SAP geometry for the heaviest Ln^{III} ions, while for the large lanthanides an equilibrium in solution exist involving both the SAP and the TSAP isomers.

The interconversion between the TSAP and the SAP isomers has been investigated for several [Ln(dota)(H$_2$O)]$^-$ complexes and related systems by means of both experimental[46,53] and theoretical tools.[48,54,55] These studies have concluded that the SAP ↔ TSAP interconversion process may proceed following two different pathways: (i) inversion of the five-membered chelate rings formed upon coordination of the cyclen moiety, which leads to a ($\delta\delta\delta\delta$) ↔ ($\lambda\lambda\lambda\lambda$) conformational change; (ii) rotation of the pendant arms, which results in a $\Delta \leftrightarrow \Lambda$ configurational change. Either process alone interconverts SAP and TSAP geometries, while the combination of the two processes exchanges enantiomeric pairs.[3]

As discussed above, the ^{1}H NMR spectra of the [Lu(do3a-pic)]$^-$ and [Lu(do3a-picOMe)]$^-$ complexes are well resolved at 298 K. Upon increasing the temperature the proton signals due to the −CH$_2$− protons of the ligand gradually broaden, reflecting dynamic intramolecular exchange processes. This is the case, for instance, of the signals due to the H7 protons of [Lu(do3a-pic)]$^-$ at 4.20 and 4.13 ppm, which gradually broaden above room temperature and finally coalesce at ca. 308 K (Figure S5, Supporting Information). From the coalescence temperature of these two signals, the barrier for the dynamic process responsible for line broadening was estimated to be $\Delta G^{\ddagger} = 70 \pm 5$ kJ·mol^{-1}. Furthermore, the proton signal due to H18ax protons of an acetate arm at 1.97 ppm does not overlap with other ^{1}H NMR signals, which allowed us to perform band-shape analysis. Indeed, if it is assumed that the exchange process associated with the line broadening (before coalescence) is slow on the actual NMR time scale, then the exchange rate for this dynamic process (k) can be calculated from $\Delta\nu_{1/2}$, the observed line widths at half-height: $k = \pi(\Delta\nu_{1/2} - \Delta\nu_{1/2}(0))$, where $\Delta\nu_{1/2}(0)$ is the line width in the absence of exchange. The Eyring plot ($R^2 > 0.9991$, Figure S5, Supporting Information) of ln(k/T) vs 1/T, where k is given in eq 9 [χ is the transmission coefficient assumed to be 1, k_B is the Boltzmann constant, T is the absolute temperature, k is the rate constant, and $\Delta G^{\ddagger}$, $\Delta H^{\ddagger}$, and $\Delta S^{\ddagger}$ are the activation free energy, enthalpy, and entropy, respectively] yields the following activation parameters: $\Delta G^{\ddagger} = 65 \pm 5$ kJ mol^{-1}, $\Delta H^{\ddagger} = 119 \pm 2$ kJ mol^{-1}, and $\Delta S^{\ddagger} = 181 \pm 3$ J K^{-1} mol^{-1} at 298 K.

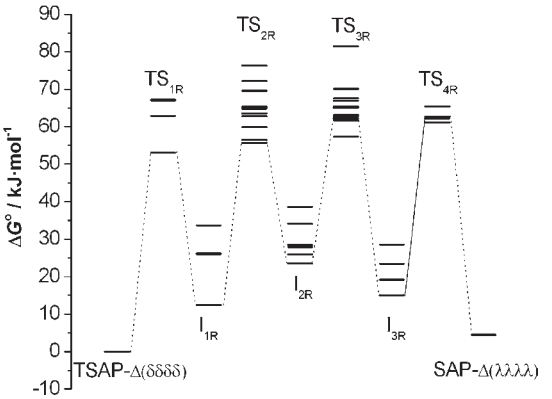

Figure 3. Relative free energies of minima, intermediates (I), and transition states (TS) involved in the ring-inversion process of [Lu(do3a-picOMe)]$^-$. The minimum energy pathway is highlighted by connecting the corresponding intermediates and transition states with dotted lines.

$$k = \chi(k_B T/h)\exp(\Delta S^{\ddagger}/R - \Delta H^{\ddagger}/RT) \qquad (9)$$

The value obtained for $\Delta G^{\ddagger}$ from this analysis is in good agreement with that obtained from the coalescence temperature of the signals due to H7 protons. In the case of [Lu(do3a-picOMe)]$^-$ a similar band shape analysis performed on the signal attributed to H18ax protons at 2.09 ppm provides the following activation parameters ($R^2 > 0.994$): $\Delta G^{\ddagger} = 67 \pm 8$ kJ mol^{-1}, $\Delta H^{\ddagger} = 135 \pm 7$ kJ mol^{-1}, and $\Delta S^{\ddagger} = 226 \pm 13$ J K^{-1} mol^{-1} at 298 K. The activation parameters obtained for the complexes of both do3a-pic^{4-} and do3a-picOMe^{4-} are very similar, pointing to a similar dynamic behavior in aqueous solution. For both Lu^{III} complexes there is a dominant diastereoisomer in solution consisting of the enantiomeric pair $\Lambda(\delta\delta\delta\delta)$ and $\Delta(\lambda\lambda\lambda\lambda)$, which provides a SAP coordination environment. The concentration of the other enantiomeric pair [$\Lambda(\lambda\lambda\lambda\lambda)/\Delta(\delta\delta\delta\delta)$] is so low that its presence in solution could not be detected by NMR. Thus, the dynamic process responsible for the broadening of the proton signals must correspond to the $\Lambda(\delta\delta\delta\delta) \leftrightarrow \Delta(\lambda\lambda\lambda\lambda)$ enantiomerization, which involves both arm rotation and ring-inversion paths.

Aiming to obtain a deeper understanding of the dynamic processes occurring in this family of complexes, we performed a detailed investigation of the arm rotation and cyclen inversion processes in the La^{III} and Lu^{III} complexes of do3a-pic^{4-} and do3a-picOMe^{4-}. According to our results obtained on B3LYP/6-31G(d)-optimized geometries in aqueous solution, inversion of the cyclen moiety is a four-step process (Figure 3). This is in line with previous computational studies performed on different Ln^{III} and Y^{III} dota-like complexes.[54−56] In each of these steps one five-membered chelate ring changes its configuration from δ to λ, passing through a transition state (TS) in which the chelate ring adopts a nearly planar conformation with the NCCN moiety in eclipsed disposition. As discussed in previous papers[54] for a molecule belonging to the C_1 point group the first step of the ring-inversion process may proceed through any of the four five-membered chelate rings of the cyclen moiety. Thus, inversion of the first chelate ring leads to four possible intermediates through

dx.doi.org/10.1021/ic2001915 |Inorg. Chem. 2011, 50, 4125–4141

Table 4. Relative Free Energies [kJ·mol^{-1}] of Minima, Intermediates (I), and Transition States (TS) Involved in the Ring-Inversion Process of [Ln(do3a-pic)]$^-$ and [Ln(do3a-picOMe)]$^-$ Complexes (Ln = La or Lu)[a]

		La			Lu	
		do3a-pic	do3a-picOMe		do3a-pic	do3a-picOMe
TSAP	Δ(δδδδ)	0.00	0.00	Δ(δδδδ)	0.00	0.00
TS_{1R}	Δ(ααXδ)	54.56	56.53	Δ(ααXδ)	55.77	53.05
I_{1R}	Δ(ααλδ)	19.33	16.32	Δ(ααλδ)	13.39	12.47
TS_{2R}	Δ(αXλδ)	63.56	63.35	Δ(αXλδ)	56.57	56.40
I_{2R}	Δ(αλλδ)	28.74	29.75	Δ(αλλδ)	23.22	23.56
TS_{3R}	Δ(αλλX)	60.63	60.96	Δ(Xλλδ)	61.92	62.63
I_{3R}	Δ(αλλλ)	26.19	24.90	Δ(λλλδ)	16.57	15.02
TS_{4R}	Δ(Xλλλ)	76.11	76.11	Δ(λλλX)	62.80	62.22
SAP	Δ(λλλλ)	17.82	19.29	Δ(λλλλ)	5.35	4.48

[a] A nearly planar conformation with the NCCN moiety in the eclipsed disposition is denoted as X; only the energies of minima and transition states that provide the lowest energy path are given.

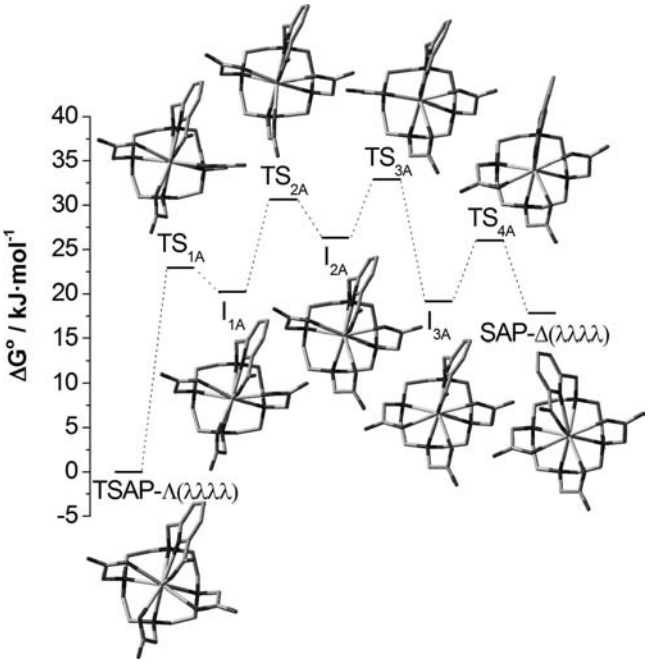

Figure 4. Relative free energies of minima, intermediates (I), and transition states (TS) involved in the arm-rotation process of [La(do3a-pic)]$^-$.

four different transition states (TSs). Inversion of a second chelate ring leads to formation of six potential intermediates. However, there are up to 12 transition states connecting intermediates I_{1R} and I_{2R}. Inversion of a third chelate ring gives rise to formation of four new intermediates (I_{3R}, Figure 3) through 12 possible TSs. Finally, inversion of the fourth chelate ring converts intermediates I_{3R} into the Δ(λλλλ) isomer. Assuming the rate-determining step for the ring-inversion process to be passage between I_{3R} and the SAP isomer (Table 4), the barrier for the ring-inversion path is the one associated to TS_{4R}, which amounts to 76 ([La(do3a-pic)]$^-$ and [La(do3a-picOMe)]$^-$), 63 ([Lu(do3a-pic)]$^-$), and 62 kJ·mol^{-1} ([Lu(do3a-picOMe)]$^-$).

Table 5. Relative Free Energies (kJ·mol^{-1}) of Minima, Intermediates (I), and Transition States (TS) Involved in the Arm Rotation Process of [Ln(do3a-pic)]$^-$ and [Ln(do3a-picOMe)]$^-$ Complexes (Ln = La or Lu)[a]

	La		Lu[a]	
	do3a-pic	do3a-picOMe	do3a-pic	do3a-picOMe
TSAP	0.00	0.00	0.00	0.00
TS_{1A}	22.93	23.14	33.39	35.40
I_{1A}	20.21	20.63		
TS_{2A}	30.63	31.84		
I_{2A}	26.32	25.23		
TS_{3A}	32.93	31.13		
I_{3A}	19.12	16.78		
TS_{4A}	26.02	26.65		
SAP	17.82	19.29	5.36	4.48

[a] The arm rotation process in the Lu^{III} analogues follows a one-step process (see text).

Thus, the energy barriers calculated for the ring-inversion process in do3a-pic^{4-} and do3a-picOMe^{4-} complexes are very similar. Furthermore, our calculations predict slightly higher energy barriers for the ring-inversion process for the La^{III} complexes than for the Lu^{III} ones. Similar free energy barriers have been obtained experimentally for Ln^{III} dota-like complexes.[46,53]

Our calculations on the [La(do3a-pic)]$^-$ and [La(do3a-picOMe)]$^-$ systems indicate that the arm rotation process responsible for the Λ(δδδδ) ↔ Δ(δδδδ) interconversion is also a four-step process involving stepwise rotation of each of the four pendant arms of the ligand (Figure 4, Table 5). According to our calculations the lowest energy path for the arm rotation process involves rotation of one of the acetate groups in the vicinity of the picolinate moiety to give intermediate I_{1A} through transition state TS_{1A}. Rotation of this acetate arm facilitates rotation of the neighboring acetate arm to give intermediate I_{2A}. Subsequent rotation of the remaining acetate group and the picolinate moiety results in formation of the SAP isomer. In the case of the Lu^{III} analogues our calculations indicate that the arm rotation process is a single-step process involving the concerted rotation of the four pendant arms of the ligand. Attempts to search for different intermediates such as those calculated for the La^{III} analogues failed, geometry optimizations leading systematically to the SAP or TSAP forms of the complexes. Previous HF and B3LYP calculations on the [Lu(dota)]$^-$ system revealed a similar concerted mechanism.[48,54,55] Most likely the more compact structure of the Lu^{III} complexes compared to the La^{III} analogues inhibits a stepwise rotation of the pendant arms due to steric hindrance. Indeed, the energy difference between intermediates and transition states involved in the stepwise arm rotation of the La^{III} analogues is rather small (2.7−6.9 kJ·mol^{-1}, see Figure 4), which suggests that increased steric hindrance may favor concerted rotation of the four pendant arms.

The barrier for the arm rotation path, as estimated from the energy of the transition state with the highest energy, amounts to 33 ([La(do3a-pic)]$^-$) and 32 ([La(do3a-picOMe)]$^-$) kJ·mol^{-1} (Table 5). In the case of the Lu^{III} analogues the free energy barriers are 33 and 35 kJ·mol^{-1} for complexes of do3a-pic^{4-} and do3a-picOMe^{4-}, respectively. Thus, the free energy values calculated for complexes of do3a-pic^{4-} and do3a-picOMe^{4-}

dx.doi.org/10.1021/ic2001915 |Inorg. Chem. 2011, 50, 4125–4141

are very similar, indicating that introduction of the methoxy group in the para position of the pyridine does not substantially affect the arm rotation process. Furthermore, the energy barriers calculated for the arm rotation process in La^{III} and Lu^{III} complexes do not differ substantially.

The data reported in Tables 4 and 5 show that the energy barrier associated to the arm rotation process is considerably lower than that responsible for the ring-inversion path, which in turn is very similar to those determined for different dota-like complexes both computationally and experimentally.[54,55] For both Lu^{III} complexes of do3a-pic^{4-} and do3a-picOMe^{4-} there is a dominant diastereoisomer in solution that provides a SAP coordination environment. Thus, the energy barriers calculated from NMR line-broadening data correspond to the $\Lambda(\delta\delta\delta\delta) \leftrightarrow \Delta(\lambda\lambda\lambda\lambda)$ enantiomerization, which involves both arm rotation and ring-inversion paths. According to our calculations the ring-inversion path is the rate-determining step of the enantiomerization process. The agreement between the experimental (65 and 66 kJ·mol^{-1} for [Lu(do3a-pic)]$^-$ and [Lu(do3a-picOMe)]$^-$) and the calculated (63 and 62 kJ·mol^{-1}, respectively) free energy barriers for the enantiomerization process is excellent, which supports the mechanism predicted by our calculations being basically correct. The situation is different in the case of the La^{III} analogues, as both the SAP and the TSAP diasteroisomers appear to be present in aqueous solution. Thus, a low energy barrier for the arm rotation process, which leads to a SAP ↔ TSAP interconversion, appears to be responsible for the line broadening observed in the NMR spectra of these complexes. For the Lu^{III} complexes there is one major isomer in solution, and therefore, the SAP ↔ TSAP interconversion is not expected to provide a substantial contribution to the chemical exchange and therefore to the line broadening, observed in the NMR spectra.

Formation Kinetics of [Eu(do3a-pic)]$^-$. Formation of Ln^{III} complexes of dota[6b] and dota-like macrocyclic ligands such as nota,[57] do3a and its derivatives,[7c] and trita[58] was found by several research groups to be slow. Data obtained by various techniques (UV−vis, luminescence, NMR, etc.) evidenced two consecutive reaction steps: fast formation of a di- or in some cases monoprotonated intermediate, which converts to the final complex in a slow rate-determining step. In the case of Ln^{III}−dota complexes two different intermediate species were identified.[59] In the first one, which is formed instantaneously, the lanthanide is bound to the four carboxylate groups of DOTA and to five water molecules (q = 5). This intermediate converts relatively fast into a more stable diprotonated intermediate in which two of the nitrogen atoms of the macrocycle are coordinated to the lanthanide (q = 3). Considering the protonation sequence of do3a-pic^{4-}, the structure of the intermediate is expected to be similar to the [Ln(H$_2$dota)]$^+$ species suggested for dota complexes and other diprotonated macrocyclic intermediates.

In order to obtain preliminary information about the rate of complex formation, the H$_x$do3a-pic ligand (c_{lig} = 1.40 × 10^{-4} M) was mixed with 3 equiv of Eu^{III} at pH = 4.34 and the UV−vis spectral changes were recorded in the wavelength range of 220−310 nm every 30 s after the solutions were mixed (Figure S6, Supporting Information). The spectrum of the ligand changed considerably when the Ln^{III} ion was added to the sample, which is in a good agreement with rapid formation of an intermediate complex in the initial step. The isosbestic points at 235 and 275 nm obtained for the series of spectra recorded

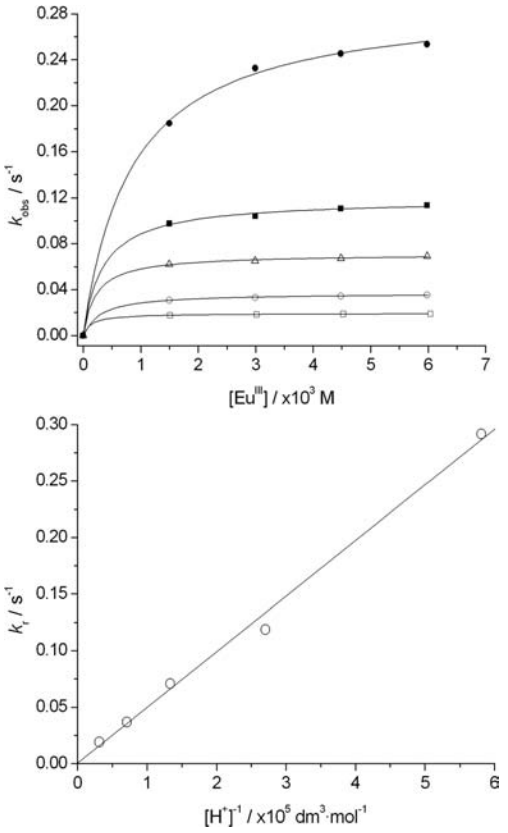

Figure 5. (Top) Pseudo-first-order rate constants, k_{obs}, as a function of Eu^{III} concentration pH = 4.50 (□), 4.85 (○), 5.12 (△), 5.43 (■), and 5.76 (●) at 25 °C, 0.1 M KCl, c_{lig} = 1.49 × 10^{-4} M. The solid lines represent the simultaneous fit of the data at all pH values to eq 13. (Bottom) Formation rate constants for [Eu(do3a-pic)]$^-$ as a function of 1/[H$^+$], 25 °C.

afterward indicate that the intermediate converts to the final product in a relatively fast reaction, which was almost complete in 300 s.

The nature of the intermediate formed in the course of the complexation reaction is often studied by direct pH measurement,[6b] that is, by measuring the pH change occurring in lightly buffered solutions upon mixing of the ligand and the metal ion. However, this method gives incorrect results when the reaction of complex formation is fast (due to the relatively long response time of the pH electrode) as well as in the case when more than one intermediate is present in solution. Hence, the indirect UV−vis method was used to approximate the composition of the intermediate since the absorbance readouts can be made considerably faster than the pH measurements. Moreover, in the case of very fast complex formation the absorbance changes during the reaction could be estimated from the kinetics curves (Abs vs time) obtained during the reaction (A_0 and A_e the absorbance readings at the beginning of the reaction and at equilibrium). The composition of the intermediate was determined by measuring the pH changes in the samples being lightly buffered with the use of an acid−base indicator (methyl orange at pH = 4.34 in the present case). The results of these experiments indicated that the intermediate was a diprotonated complex, as the number of protons released in the second step was almost twice those released during the initial step (at pH = 4.34 the ligand is in the form of H$_4$L 18%,

dx.doi.org/10.1021/ic2001915 |Inorg. Chem. 2011, 50, 4125–4141

Table 6. Stability Constants of $[Ln(H_2L)^*]$ Intermediates ($K_{[Ln(H2L)^*]}$) and k_{OH} ($M^{-1}\cdot s^{-1}$) Rate Constants Characterizing the Rearrangement of the Intermediate to the LnL Complexes, 25 °C (Ln = Eu^{III} or Gd^{III})

ligand	Ln^{III}	log $K_{[Ln\ (H2L)^*]}$	k_{OH} ($M^{-1}\cdot s^{-1}$)	ref
do3a-pic^{4-}	Eu^{III}	3.8(5)	$(3.3(2)) \times 10^7$	this work
do3a^{3-}	Gd^{III}	4.0[a]	2.1×10^7	7c
pcta^{3-}	Eu^{III}	3.1	1.7×10^8	60
do3a-hp^{3-}	Gd^{III}	3.9[a]	1.2×10^7	7c
do3a-b^{3-}	Eu^{III}	2.5	4.8×10^6	61
do3a-*N*prop^{4-}	Gd^{III}	4.5	2.9×10^7	62
dota^{4-}	Eu^{III}	4.4	1.1×10^7	6b
trita^{4-}	Gd^{III}	3.9	2.6×10^7	58

[a] Calculated from the conditional stability constant obtained at pH 4.26 and 4.28 for [Gd(do3a)] and [Gd(do3a-hp)] complexes, respectively; published by Kumar et al.[7c]

H_3L 64%, and H_2L 18%, so altogether approximately 1 equiv of protons gets released in the first step). The kinetic studies were subsequently performed at different pH values using a similar ligand concentration ($c_{lig} = 1.49 \times 10^{-4}$) and an excess of Eu^{III} ions (10−40-fold excess of the metal ion). The reactions were followed using the stopped-flow technique at 285 nm (Figure 5).

In the presence of Ln^{III} excess (pseudo-first-order conditions), the rate of the formation reaction can be expressed according to eq 10

$$\frac{d[LnL]_t}{dt} = k_{obs}[L]_0 \qquad (10)$$

where $[L]_0$ is the total concentration of the free ligand and k_{obs} is a pseudo-first-order rate constant. By plotting the k_{obs} values vs the metal ion concentration saturation curves are obtained for all pH values investigated (Figure 5). Assuming that the rate-determining step of the reaction is the slow deprotonation of the intermediate, the following expression can be applied

$$\frac{d[LnL]_t}{dt} = k_{obs}[L]_0 = k_r[Ln(H_2L)^*] \qquad (11)$$

The total concentration of the ligand, $[L]_0$, can be given as $[L]_0 = [Ln(H_2L)^*] + [L]_{free}$ ($K_{[Ln(H2L)^*]} = [Ln(H_2L)^*]/[Ln^{3+}][H_2L]$). The concentration of the free (uncomplexed) ligand is a sum of concentrations for the different protonated forms of the ligand ($[L]_{free} = [H_5L^+] + [H_4L] + [H_3L^-] + [H_2L^{2-}] + [HL^{3-}] + [L^{4-}]$). $[L]_{free}$ can be expressed using the protonation constants determined by pH-potentiometric titrations

$$[L]_{free} = [H_2L^{2-}]\left(\frac{1}{K_1^H K_2^H [H^+]^2} + \frac{1}{K_2^H[H^+]} + 1 + K_3^H[H^+] + K_3^H K_4^H[H^+]^2 + K_3^H K_4^H K_5^H[H^+]^3\right) = [H_2L^{2-}]\cdot\alpha_{H_2L} \qquad (12)$$

The concentrations of fully deprotonated and monoprotonated forms of the ligand are very low in the pH range used to investigate complex formation (4.50 − 5.78), and therefore, the contribution of the first two terms within parentheses in eq 12 can be neglected. If the sum displayed in parentheses is denoted as α_{H2L}, the following equation can derived for k_{obs}

$$k_{obs} = \frac{k_r\frac{K_{Ln(H_2L)^*}}{\alpha_{H_2L}}[Ln^{3+}]}{1 + \frac{K_{Ln(H_2L)^*}}{\alpha_{H_2L}}[Ln^{3+}]} \qquad (13)$$

The pseudo-first-order rate constants were simultaneously fitted to eq 13 at various pH values and metal ion concentrations (Figure 5), which allowed one to calculate the rate constants, k_r, and the stability constant of the diprotonated intermediate, $K_{[LnH2L^*]}$ (Table 6). The k_r values obtained in this way were found to be proportional to $1/[H^+]$, as illustrated in Figure 5. This is consistent with a general base-catalyzed mechanism, as found earlier for complexes of dota^{4-} and its derivatives.[6b,7c] Therefore, k_r in eq 13 can be expressed in terms of the relative contributions from various bases present in solution (eq 14)

$$k_r = k_{H_2O} + k_{OH}[OH^-] \qquad (14)$$

where k_{H_2O} and k_{OH} are rate constants characterizing the deprotonation involving a water-assisted (or other base) and an OH^--catalyzed deprotonation of the intermediate, respectively. By comparing the k_{H2O} and k_{OH} rate constants it can be concluded that the contribution of the pathway characterized by k_{H2O} ($0.005 \pm 0.002\ s^{-1}$) is about 10 orders of magnitude smaller than the k_{OH} rate constant, and it can therefore be safely neglected. The k_{OH} rate constants characterizing the OH^--ion-catalyzed deprotonation of the intermediate are compared to those obtained for dota and its derivatives in Table 6.

The stability constant of the $[Eu(H_2L)^*]$ intermediate is similar to those reported for the corresponding do3a, dota, and dota derivatives, while the rate constants of the OH^--catalyzed deprotonation step of the intermediate complex is slightly higher for the complex of do3a-pic than for dota and dota-like analogues. The data reported in Table 6 indicate that replacement of one acetate arm of dota by a picolinate unit results in 3-fold increase in the formation rate of Eu^{III} complexes. This increase is slightly higher than what was observed recently for the do3a-*N*prop ligand by É. Tóth and co-workers,[62] which is very likely a consequence of the presence of a somewhat more rigid picolinate moiety.

Acid-Catalyzed Dissociation of [Ln(do3a-pic)]$^-$ Complexes (Ln = Ce, Eu, and Yb). Dissociation of the complexes in vivo may occur through one of the following pathways:[63] (1) proton-independent dissociation characterized by the rate constant k_{LnL} (often referred as spontaneous dissociation and denoted as k_0), (2) proton-assisted dissociation characterized with the protonation constants K_{LnHL} and K_{LnH2L} and rate constants k_{LnHL} and k^H_{LnHL} (often marked as k_1 and k_2), (3) ligand-assisted dissociation characterized by the stability constant of mixed ligand complexes K_{LLnL^*} and rate constant k_{LLnL^*}, and (4) metal-ion-catalyzed dissociation characterized by the stability of dinuclear complexes K_{LnLM} (where M = Zn, Cu, or Eu) and rate constant k_{LnLM} (often expressed as $k^M{}_3$). Dissociation of complexes of dota-based macrocyclic ligands often occurs very slowly because their tightly packed and highly rigid structure results in high kinetic inertness of such complexes. As a consequence, the rate constants k_{LnL}, k_{LLnL^*}, and k_{LnLM} are often very small, the acid-catalyzed process being the main dissociation pathway for the complexes of this class.[6]

dx.doi.org/10.1021/ic2001915 |*Inorg. Chem.* 2011, 50, 4125–4141

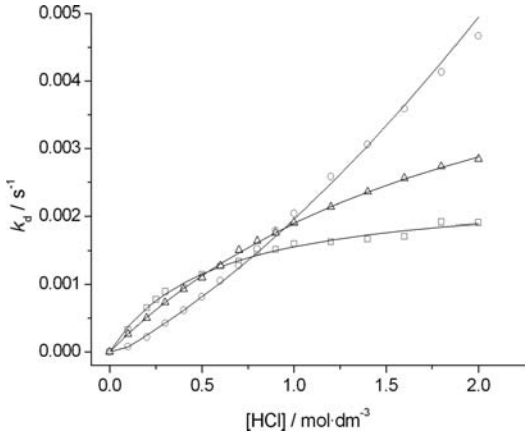

Figure 6. Dissociation rates (k_d) for $[Ln(do3a\text{-}pic)]^-$ complexes (Ln = Ce (□), Eu (○), and Yb (△)) as a function of the H^+ concentration. The solid lines represent the fits of the data to eq 16 (Eu^{III}) or 17 (Ce^{III} and Yb^{III}).

The acid-catalyzed dissociation rates of $[Ln(do3a\text{-}pic)]^-$ complexes (Ln = Ce^{III}, Eu^{III}, and Yb^{III}) have been studied with the use of acid solutions (0.1−2.0 M HCl). Under these conditions the complexes are thermodynamically unstable and dissociate completely. The rates of dissociation can be expressed by eq 15

$$-\frac{d[LnL]_t}{dt} = k_d[LnL]_t \qquad (15)$$

Plots of the obtained k_d values vs H^+ concentration for the different complexes are shown in Figure 6. In general, two types of curves are observed when the rate constants are plotted against the acid concentration. For the Ce^{III} and Yb^{III} complexes the rates show saturation curves, while for the Eu^{III} complex the plot indicates a quadratic dependence with proton concentration (with a small contribution from k_2). The saturation behavior of the curves can be explained by the presence of an intermediate, a protonated complex, forming rapidly at the beginning of the reaction. This behavior has also been observed for the $[Eu(dota)]^-$ complex[6b] as well as for the Ln^{III} complexes of the rigidified macrocyclic pcta ligand.[60] The quadratic dependence on acid concentration has been observed fewer times for complexes of macrocyclic ligands but more often occurs for complexes of open chain dtpa (diethylenetriamine pentaacetic acid) derivatives. However, the acid-catalyzed dissociation of $[Ce(dota)]^-$ and the Ce^{III} complex of the structurally similar ligand H_2bp12c4 show this behavior.[64,14c] A quadratic dependence with proton indicates that dissociation might take place by both the proton-independent (characterized by k_0) and the proton-assisted pathways, presumably with formation and dissociation of mono- and diprotonated complexes (characterized by k_1 and k_2, respectively). Thus, the observed first-order dissociation rate constants were fitted to eq 16 (Eu^{III}) or 17 (Ce^{III} and Yb^{III})

$$k_d = k_0 + k_1[H^+] + k_2[H^+]^2 \qquad (16)$$

$$k_d = \frac{k_0 + k_1K_1^H[H^+]}{1 + K_1^H[H^+]} \qquad (17)$$

The k_0 values obtained from the least-squares fit of the rate constants have been found to be either small negative values (the case of Ce^{III} and Eu^{III}) or, in the case of Yb^{III}, a small positive value with a large error (6 times larger than k_0 itself ($k_0 = 1.1 \pm 6.7 \times 10^{-6}$ s^{-1})). However, this is not very surprising since under our experimental conditions the acid-independent dissociation is not a major dissociation pathway and hence can be neglected, as dissociation mainly occurs through the acid-catalyzed pathway. The results obtained from the fittings are summarized in Table 7.

Table 7. Comparison of Acid-Assisted Dissociation Rate Constants (k_1, $M^{-1}\cdot s^{-1}$) for $[Ln(do3a\text{-}pic)]^-$ Complexes (I = 0.1 M KCl, 25 °C) (data for related systems provided for comparison)

ligand	Ce^{III}	Eu^{III}	Gd^{III}	Yb^{III}
$do3a\text{-}pic^{4-}$	$2.40(6) \times 10^{-3}$ [a]	$1.56(7) \times 10^{-3}$ [b]		$2.79(3) \times 10^{-3}$ [a]
$do3a^{3-}$ [a,c]	1.12×10^{-1}		2.7×10^{-2}	2.8×10^{-2}
			1.17×10^{-2} [d]	
			5.2×10^{-2} [e]	
$pcta^{3-}$ [f]	9.6×10^{-4} [g]	5.1×10^{-4}	1.1×10^{-3} [f,h]	3.9×10^{-4} [a]
				2.8×10^{-4} [g]
$dota^{4-}$ [i]	8×10^{-4} [j]	1.4×10^{-5} [k]	2.0×10^{-5} [l]	
			8.4×10^{-6} [m]	

[a] Calculated from saturation kinetics. [b] Second-order dependence on H^+ ion concentration with third-order rate constant $(4.8 \pm 0.8) \times 10^{-4}$ M^{-2} s^{-1} was also observed. [c] From ref 65. [d] From ref 66. [e] Data corresponding to the Y^{III} complex. [f] From ref 60. [g] Calculated from saturation kinetics obtained in a wide acid concentration range. [h] Second-order dependence on H^+ ion concentration with third-order rate constant $5.7 \pm 0.4 \times 10^{-5}$ M^{-2} s^{-1} was also observed. [i] From ref 7b. [j] Second-order dependence on H^+ ion concentration with third-order rate constant 2.0×10^{-3} M^{-2} s^{-1} was also observed in ref 64. [k] From ref 6b. [l] At 37 °C, ref 6b. [m] Reference 6a

As it can be seen from Table 7 replacement of one acetate moiety in dota by a picolinate side arm resulted in a significant increase in the rates of acid-catalyzed dissociation. This can be explained by the presence of an extra donor atom that can be easily protonated (for $[Ln(do3a\text{-}pic)]^-$ stable protonated complexes were observed with log K_1^H values ranging from 2.48 to 2.72). However, these rates are 1−2 orders of magnitude lower than those of the identical do3a analogues and 3 orders of magnitude lower than those observed for the Ln^{III} complexes of H_2bp12c4. Thus, the $do3a\text{-}pic^{4-}$ complexes are remarkably inert with respect to metal ion dissociation.

CONCLUSIONS

In this work we have shown that the Ln^{III} complexes of $do3a\text{-}pic^{4-}$ have a number of interesting properties that include (i) a high thermodynamic stability, which for the large lanthanides is comparable to that of the dota analogues, (ii) relatively fast kinetics of complexation in comparison to the dota derivatives, (iii) remarkable inertness with respect to metal ion dissociation, and (iv) high luminescence quantum yields of the Eu^{III} and Tb^{III} complexes due to an efficient shielding of the metal ions from the surrounding water molecules.

A detailed investigation of the structure and dynamics of the complexes in solution shows that the complexes of the light Ln^{III} ions exist in solution as a mixture of the SAP and TSAP isomers, while for the heaviest lanthanides the SAP form could be detected in solution. Analysis of the Yb^{III}-induced paramagnetic shifts unambiguously demonstrates that this complex has SAP coordination in solution. For the heaviest Ln^{III} ions

the rate-determining step for the $\Lambda(\delta\delta\delta\delta) \leftrightarrow \Delta(\lambda\lambda\lambda\lambda)$ enantiomerization corresponds to the ring-inversion pathway, the arm rotation process possessing lower activation barriers. A low-energy barrier for the arm rotation process, which leads to a SAP ↔ TSAP interconversion, appears to be responsible for the line broadening observed in the NMR spectra of the La^{III} complexes.

Introduction of a methoxy group in the 4 position of the pyrididyl unit of do3a-pic^{4-} does not have an important effect on the structure and dynamics of the corresponding Ln^{III} complexes in solution. However, the photophysical properties of the complexes are dramatically affected, the luminescence quantum yield of the europium complexes dropping from 24% for [Eu(do3a-pic)]$^-$ to 9% for [Eu(do3a-picOMe)]$^-$. These results show that the photophysical properties of the Eu^{III} complexes can be tuned by changing the substituents attached to the 4 position of the pyridyl unit. On the basis of these data, do3a-pic^{4-} seems to be an attractive structural platform for constructing Ln^{III}-based luminescent probes.

EXPERIMENTAL SECTION

General Methods. Elemental analyses were carried out on a Carlo Erba 1108 elemental analyzer. High-resolution ESI-TOF mass spectra were recorded using a LC-Q-q-TOF Applied Biosystems QSTAR Elite spectrometer in the negative mode. IR spectra were recorded using a Bruker Vector 22 spectrophotometer equipped with a Golden Gate Attenuated Total Reflectance (ATR) accessory (Specac). ^{1}H and ^{13}C NMR spectra were recorded at 25 °C on Bruker Avance 300 and Bruker Avance 500 MHz spectrometers. For measurements in D_2O, *tert*-butyl alcohol was used as an internal standard with the methyl signal calibrated at δ = 1.2 (^{1}H) and 31.2 ppm (^{13}C). Spectral assignments were based in part on two-dimensional COSY, EXSY, HSQC, and HMBC experiments.

Absorption and Emission Spectra. UV−vis absorption spectra were recorded on a Specord 205 (Analytikjena) spectrometer. Emission and excitation spectra were recorded on a Horiba Jobin Yvon Fluorolog 3 spectrometer equipped with a continuous 450 W Xe lamp and corrected for variations of the lamp intensity and for the wavelength dependence of the photomultiplier response. Luminescence decays were obtained on the same instrument with an "ozone-free" Xe flash lamp over temporal windows covering at least five decay times. Luminescence quantum yields were measured according to conventional procedures,[67] with diluted solutions (optical density <0.05), using $[Ru(bipy)_3]Cl_2$ in nondegassed water (Φ = 2.8%)[68] and rhodamine 6G in water (Φ = 76% at λ_{exc} = 488 nm),[69] with an estimated error of ±15%. Hydration numbers, q, were obtained using eq 18, where τ_{H_2O} and τ_{D_2O}, respectively, refer to the measured luminescence decay lifetime (in milliseconds) in water or deuterated water. Given values are the average of values obtained with A = 1.11 and B = 0.31[35a] and A = 1.2 and B = 0.25[35c] for Eu and with A = 5 and B = 0.06[35c] and A = 4.2 and B = 0[35b] for Tb (estimated error ±0.5 water molecules)

$$q = A \times [(1/\tau_{H_2O} - 1/\tau_{D_2O}) - B] \quad (18)$$

Potentiometric Measurements. The stock solutions of $LnCl_3$ (Ln = La, Ce, Eu, Gd, Yb, and Lu) were prepared by dissolving lanthanide(III) oxides in concentrated HCl (taken in a slight excess). The excess HCl acid was removed by repeated evaporation to dryness until the pH of the solution was no longer very acidic (pH = 4.0−5.5). The concentrations of the stock solutions were determined by complexometric titration using a standardized Na_2H_2EDTA solution in the presence of xylenol orange as an indicator. The Na_2H_2EDTA solution was standardized with a $ZnCl_2$ stock solution (prepared by dissolving metallic Zn (99.9%, Merck) in diluted HCl solution and using eriochromeblack T indicator). The stock solution of the do3a-pic ligand was prepared by dissolving m = 0.4663 g of the ligand in 50.0 mL of double-distilled water and subsequent filtration through membrane filter (0.45 μM) due to the slight opalescence of the stock solution. The concentration of the ligand in the stock solution as well as the amount of the excess of acid in the sample (C_{H+}/C_L) was determined by pH-potentiometric titration. For concentration determinations, solutions of the ligand were titrated with 0.2152 M KOH in the absence and presence of a large excess of Ca^{II} ($C_{Ca}{}^{II}/C_L$ ratio was approximately 50), when all dissociable protons dissociate. The pH of the sample solutions were set to about 1.75−1.80 before the pH-potentiometric titrations with a measured volume of strong acid (HCl) of known concentration. The protonation constants of the ligand were calculated from the data obtained by titrating 1.4 and 2.8 mM ligand samples (total 660 data pairs) with standardized KOH solution (0.2152 M) in the absence of Ca^{II} over the pH range of 1.75−11.80.

The pH-potentimetric titrations were carried out with the Methrohm 785 DMP Titrino system using a Metrohm combination microelectrode (6.0234.100) in a vessel being mechanically stirred and thermostatted at 25.0 °C. Autoburet of 5 mL capacity was used for base additions. The ionic strength in the samples was set to 0.1 M using KCl. All equilibrium measurements (direct titrations) were carried out in 6.00 mL sample volumes. During the titrations, N_2 gas was bubbled through samples to maintain the cell free of CO_2. Standard buffers (0.01 M borax, pH = 9.180 and 0.05 M KH−phthalate, pH = 4.007) were used to calibrate the electrode. The titrant, a carbonate-free KOH solution, was standardized against 0.05 M KH−phthalate solution by pH-potentiometric method. The method proposed by Irving et al.[70] was used to obtain H^+ ion concentrations from the measured pH values; therefore, "stoichiometric" constants were determined. The ionic product of water, pK_w, was also calculated from these titration data and found to be 13.798.

Owning to the relatively slow rates of complexation involving Ln^{III} ions and macrocyclic ligands, the stability constants were determined with the use of the "out-of-cell" (also known as the batch method) technique (pH-potentiometry). Fourteen 1.5 mL samples containing known amounts of ligand and Ln^{III} were prepared with known and varying added acid concentration, so that the pH was adjusted to a range where complexation could be expected to take place. The samples were sealed under a blanket of N_2 and kept in an incubator at 25 °C for 2−3 weeks. The latter (or required minimum) time period to reach equilibrium was established by preliminary spectrophotometric studies on duplicates of the most acidic and most basic samples kept together with the rest of the "out-of-cell" samples. The samples were then opened, and the equilibrium pH was measured with the use of a Radimeter PHM 93 pH meter equipped with a Metrohm combined microelectrode (6.0234.100). The software PSEQUAD[71] was used to process the titration data, i.e., to calculate the protonation and stability constants expressed by eqs 1−3. The reliability of the constants are characterized by the calculated standard deviation values shown in parentheses and the fitting of parameter values (ΔV, which is the difference between the experimental and the calculated titration curves expressed in milliliters of the titrant).

Formation and Dissociation Kinetics of Some [Ln(do3a-pic)]$^-$ Complexes. Formation rates of [Eu(do3a-pic)]$^-$ (λ_{max} = 285 nm) were determined at 25 °C and 0.1 M KCl ionic strength by spectrophotometry using either a Varian Cary 1E UV−vis spectrophotometer (conventional method for the samples with pH < 4.8) equipped with thermostatted cell holders and semimicro quartz cells (Hellma, optical path length 1 cm) or a stopped-flow method with an Applied Photophysics DX-17MV instrument. All reactions were performed under pseudo-first-order conditions where the metal ion was in 10−40-fold excess and the concentration of the ligand was set to 1.49 ×

dx.doi.org/10.1021/ic2001915 |Inorg. Chem. 2011, 50, 4125–4141

10^{-4} M. Formation kinetic studies were carried out with noncoordinating buffers, *N*-ethylpiperazine (NEP, log K_2^H = 5.55) and dimethylpiperazine (DMP, log K_2^H = 4.72) at 0.025 M concentration to maintain constant pH in the pH range of 4.50−5.76.

Absorbance data recorded as a function of time were fitted to eq 19 to evaluate the first-order rate constants with Scientist (Micromath) software using a standard least-squares procedure (A_0, A_e, and A_t are the absorbance values measured at the start of the reaction (t = 0), at equilibrium condition, and at time t, respectively)

$$A_t = A_e + (A_0 - A_e)\cdot e^{(-k\cdot t)} \quad (19)$$

The relative error for fitting of the absorbance vs time data was less than 1%, while the calculated first-order rate constants (k_{obs}) were reproduced to within 2−3% error as determined in 4−6 parallel experiments (each point in Figure 5 reflects an average of 4−6 kinetic runs obtained under identical conditions).

Proton-assisted dissociation kinetics were studied under pseudo-first-order conditions in acidic solutions (0.05−2.0 M HCl) at 25 °C and 2.0 M ionic strength provided by $(K^+ + H^+)Cl^-$ in samples where the concentration of complexes was 0.139 (Ce), 0.139 (Eu), and 0.141 (Yb) mM. Under these conditions the complexes are not stable and dissociate fully. The decrease in absorbance was measured periodically at 285 nm by following the changes in the $\pi \rightarrow \pi^*$ transition of the ligand chromophore (i.e., the picolinate moiety). Throughout the time period elapsed for the mixing of the reactants (usually 5−6 s) no evidence of significant amplitude loss was observed. The changes in the absorbance were followed until 100% conversion (complete) was reached, and the kinetic curves were fitted to eq 19 (i.e., single-exponential decay) with excellent confidence.

Chemicals and Starting Materials. 6-Chloromethylpyridine-2-carboxylic acid methyl esther (**4a**) was prepared according to the literature method.[14a] All other chemicals were purchased from commercial sources and used without further purification, unless otherwise stated. Silica gel (Fluka 60, 0.063−0.2 mm) and neutral Al_2O_3 (Fluka, 0.05−0.15 mm) were used for preparative column chromatography.

Dimethyl 4-Methoxypyridine-2,6-dicarboxylate (2b). This compound was prepared using a slight modification of the literature procedure.[39] 4-Hydroxypyridine-2,6-dicarboxylic acid (15.0 g, 81.9 mmol) was dissolved in methanol (300 mL), and 25 mL of concentrated H_2SO_4 was added. The mixture was heated to reflux with stirring for a period of 24 h and then allowed to cool to room temperature. A saturated $NaHCO_3$ solution was added (200 mL), and the mixture was extracted with CH_2Cl_2 (5 × 300 mL). The combined organic extracts were dried over $MgSO_4$ and evaporated to dryness. The crude product was purified by column chromatography on SiO_2 with a CH_2Cl_2/MeOH 10% mixture as the eluent to give 14.6 g of **2b** as a white solid. Yield 79%. Anal. Calcd for $C_{10}H_{11}NO_5$: C, 53.33; H, 4.92; N, 6.22. Found: C, 53.05; H, 4.82; N, 6.13. MS (ESI$^+$): m/z 226 ($[C_{10}H_{12}NO_5]^+$). IR (ATR, cm^{-1}): ν 1713 (C═O), 1602 (C═N). ^{1}H NMR ($CDCl_3$, 500 MHz, 20 °C, TMS): δ 7.82 (d, 2H, py), 4.01 (s, 6H, −$COOCH_3$), 3.98 (s, 3H, py, −OCH_3). ^{13}C NMR ($CDCl_3$, 125.8 MHz, 20 °C, TMS): δ 167.6, 165.1, 149.8, 114.1, 56.0, 53.2.

Methyl 6-(Hydroxymethyl)-4-methoxypicolinate (3b). $NaBH_4$ (9.1 g, 0.24 mol) was added in small portions over a period of 0.5 h to a stirred solution of **2b** (14.6 g, 64.8 mmol) in MeOH (500 mL) at 0 °C. The mixture was stirred at 0 °C for 3 h, and then a saturated $NaHCO_3$ aqueous solution (200 mL) was added. The resulting solution was extracted with CH_2Cl_2 (5 × 200 mL), and the combined organic extracts were dried over Na_2SO_4 and evaporated to give 9.6 g of **3b** as a white solid. Yield 75%. Anal. Calcd for $C_9H_{11}NO_4$: C, 54.82; H, 5.62; N, 7.10. Found: C, 54.67; H, 5.80; N, 7.15. MS (ESI$^+$): m/z 198 ($[C_9H_{12}NO_4]^+$). IR (ATR, cm^{-1}): ν 1739 (C═O), 1600 (C═N). ^{1}H NMR ($CDCl_3$, 500 MHz, 20 °C, TMS): δ 7.53 (d, 1H, py, ^4J = 2.4 Hz), 7.06 (d, 1H, py, ^4J = 2.4 Hz), 4.79 (s, 2H, py, CH_2OH), 3.96 (s, 3H, −$COOCH_3$), 3.90 (s, 3H, −OCH_3). ^{13}C NMR ($CDCl_3$, 125.8 MHz, 20 °C, TMS): δ 167.2, 165.5, 162.3, 148.5, 110.6, 109.2, 64.6, 55.6, 52.9.

Methyl 6-(Chloromethyl)-4-methoxypicolinate (4b). $SOCl_2$ (5 mL) was added over **3b** (1.00 g, 5.07 mmol) at 0 °C under an inert atmosphere (Ar). The mixture was stirred at 0 °C for 4 h, and the excess of $SOCl_2$ was removed under reduced pressure. The residue was dissolved in toluene (50 mL), and the organic solution was washed with a 1 M $NaHCO_3$ aqueous solution. The organic extract was evaporated, and the resulting oily residue was purified by column chromatography on SiO_2 with a hexane/AcOEt 3:2 mixture as the eluent to give 0.93 g of **4b** as a yellow solid. Yield 85%. Anal. Calcd for $C_9H_{10}ClNO_3$: C, 50.13; H, 4.67; N, 6.50. Found: C, 50.05; H, 4.52; N, 6.48. MS (ESI$^+$): m/z 216 ($[C_9H_{11}ClNO_3]^+$). IR (ATR, cm^{-1}): ν 1714 (C═O), 1597 (C═N). ^{1}H NMR ($CDCl_3$, 500 MHz, 20 °C, TMS): δ 7.60 (d, 1H, py, ^4J = 2.4 Hz), 7.22 (d, 1H, py, ^4J = 2.4 Hz), 4.72 (s, 2H, CH_2Cl), 4.00 (s, 3H, −$COOCH_3$), 3.94 (s, 3H, −OCH_3). ^{13}C NMR ($CDCl_3$, 125.8 MHz, 20 °C, TMS): δ 167.5, 165.3, 158.7, 149.0, 111.8, 110.8, 55.7, 53.1, 46.2.

Tri-*tert*-butyl 2,2′,2″-(10-((6-(Methoxycarbonyl)pyridin-2-yl)methyl)-1,4,7,10-tetraazacyclododecane-1,4,7-triyl)triacetate (5a). Compound **4a** (0.210 g, 1.13 mmol) and Na_2CO_3 (0.60 g, 5.65 mmol) were added to a solution of do3a(*t*-BuO)$_3$ (0.580 g, 1.13 mmol) in acetonitrile (25 mL). The mixture was heated to reflux with stirring for a period of 24 h, and then the excess of Na_2CO_3 was filtered off. The filtrate was concentrated to dryness, and the yellow residue was extracted with 10 mL of a H_2O and CH_2Cl_2 (1:3) mixture. The organic phase was evaporated to dryness to give an oily residue that was purified by column chromatography on Al_2O_3 with a CH_2Cl_2/MeOH 5% mixture as the eluent to give 0.71 g of **5a** as a yellow oil. Yield 84%. Anal. Calcd for $C_{34}H_{57}N_5O_8\cdot CH_2Cl_2$: C, 56.14; H, 7.94; N, 9.35. Found: C, 55.85; H, 7.78; N, 9.13. MS (ESI$^+$): m/z 664 ($[C_{34}H_{58}N_5O_8]^+$). IR (ATR, cm^{-1}): ν 1720 (C═O), 1591 (C═N). ^{1}H NMR ($CDCl_3$, 500 MHz, 20 °C, TMS): δ 7.99 (d, 1H, py, ^3J = 7.7 Hz), 7.92 (m, 1H, py), 7.56 (d, 1H, py, ^3J = 7.7 Hz), 5.29 (s, CH_2Cl_2), 3.89 (s, 3H, −OCH_3), 3.18−2.37 (m, 24H, −CH_2−), 1.47 (s, 9H, *t*-BuO−), 1.31 (s, 18H, *t*-BuO−). ^{13}C NMR ($CDCl_3$, 125.8 MHz, 20 °C, TMS): δ 172.1, 171.1, 165.2, 159.1, 146.4, 138.3, 127.2, 123.5, 82.1, 81.8, 59.1, 56.1, 55.8, 53.4, 52.7, 51.2, 50.4, 28.0, 27.9.

Tri-*tert*-butyl 2,2′,2″-(10-((4-Methoxy-6-(methoxycarbonyl)pyridin-2-yl)methyl)-1,4,7,10-tetraazacyclododecane-1,4,7-triyl)triacetate (5b). The synthesis of this compound followed the same procedure described for **5a** but using **4b** (0.250 g, 1.16 mmol) instead of **4a**. Yield 0.81 g, 90%. Anal. Calcd for $C_{35}H_{59}N_5O_9\cdot CH_2Cl_2$: C, 55.52; H, 7.89; N, 8.99. Found: C, 55.65; H, 7.67; N, 9.15. MS (ESI$^+$): m/z 716 ($[C_{35}H_{59}N_5NaO_9]^+$). IR (ATR, cm^{-1}): ν 1722 (C═O), 1600 (C═N). ^{1}H NMR ($CDCl_3$, 500 MHz, 20 °C, TMS): δ 7.50 (d, 1H, py, ^4J = 2.4 Hz), 7.14 (d, 1H, py, ^4J = 2.4 Hz), 5.29 (s, CH_2Cl_2), 3.96 (s, 3H, −$COOCH_3$), 3.89 (s, 3H, OCH_3), 3.17−2.04 (m, 24H, −CH_2−), 1.48 (s, 9H, *t*-BuO−), 1.34 (s, 18H, *t*-BuO−). ^{13}C NMR ($CDCl_3$, 125.8 MHz, 20 °C, TMS): δ 172.1, 171.3, 167.4, 165.1, 160.8, 147.9, 110.9, 110.8, 82.1, 81.8, 56.0, 55.8, 55.6, 53.4, 52.4, 51.6, 50.2, 50.0, 28.0, 27.9.

2,2′,2″-(10-((6-Carboxypyridin-2-yl)methyl)-1,4,7,10-tetraazacyclododecane-1,4,7-triyl)triacetic Acid (H_4do3a-pic). A solution of compound **5a** (0.710 g, 0.95 mmol) in 6 M HCl (20 mL) was heated to reflux for 24 h, and then the solvent was removed in a rotary evaporator to give a yellow oil. A small amount of MeOH was added (∼10 mL) and the mixture evaporated to dryness. This process was repeated once with addition of MeOH and twice with addition of diethyl ether (∼10 mL) to give 0.610 g of the desired ligand as a pale yellow solid. Yield 87%. Anal. Calcd for $C_{21}H_{31}N_5O_8\cdot 5HCl\cdot 4H_2O$: C, 34.28; H, 6.03; N, 9.52. Found: C, 34.50; H, 5.43; N, 9.47. MS (ESI$^+$): m/z 482 ($[C_{21}H_{32}N_5O_8]^+$). IR (ATR, cm^{-1}): ν 1721 (C═O), 1617 (C═N). ^{1}H NMR (D_2O, pD 7.0, 500 MHz, 20 °C, TMS): δ 7.92

(m, 2H, py), 7.85 (m, 1H, py), 3.99−2.91 (m, 24H, CH_2). ^{13}C NMR (D_2O, pD 7.0, 125.8 MHz, 20 °C, TMS): δ 177.9, 173.3, 171.2, 156.9, 153.5, 142.4, 128.7, 124.9, 59.4, 57.8, 56.5, 53.1, 52.1, 49.7, 49.5.

2,2′,2″-(10-((6-Carboxy-4-methoxypyridin-2-yl)methyl)-1,4,7,10-tetraazacyclododecane-1,4,7-triyl)triacetic Acid (H_4do3a-picOMe). A solution of compound **5b** (0.810 g, 1.04 mmol) in 6 M HCl (20 mL) was heated to reflux for 24 h, and then the solvent was removed in a rotary evaporator to give a yellow oil. A small amount of MeOH was added (∼10 mL) and the mixture evaporated to dryness. This process was repeated once with addition of MeOH and twice with addition of diethyl ether (∼10 mL) to give 0.720 g of the desired ligand as a pale yellow solid. Yield 93%. Anal. Calcd for $C_{22}H_{33}N_5O_9 \cdot 5HCl \cdot 3H_2O$: C, 35.33; H, 5.93; N, 9.36. Found: C, 35.57; H, 5.46; N, 9.16. MS (ESI$^+$): m/z 512 ($[C_{22}H_{34}N_5O_9]^+$). IR (ATR, cm^{-1}): ν 1723 (C═O), 1620 (C═N). ^1H NMR (D_2O, pD 7.0, 500 MHz, 20 °C, TMS): δ 7.64 (m, 1H, py), 7.54 (m, 1H, py), 4.03 (s, 3H, -OCH_3), 4.02−2.94 (m, 24H, CH_2). ^{13}C NMR (D_2O, pD 7.0, 125.8 MHz, 20 °C, TMS): δ 178.2, 172.9, 171.0, 168.9, 155.8, 152.4, 115.4, 113.1, 59.0, 57.8, 56.9, 56.8, 53.2, 51.9, 49.7, 49.6.

General Procedure for Preparation of (Et_3NH)[Ln(do3a-pic)] Complex Salts. A mixture of do3a-pic·5HCl·4H_2O (0.100 g, 0.136 mmol), triethylamine (0.138 g, 1.36 mmol), and Ln(OTf)$_3$ (0.136 mmol, Ln = La, Eu, Gd, Tb, Yb, or Lu) in 2-propanol (15 mL) was heated to reflux for 24 h. The reaction was allowed to cool to room temperature and then concentrated to dryness. Addition of THF (5 mL) resulted in formation of a white precipitate, which was isolated by filtration. The solid was then suspended in 10 mL of THF and stirred at room temperature for 24 h. The solid was isolated by filtration, washed with THF and diethyl ether, and dried under vacuum.

(Et_3NH)[La(do3a-pic)]. Yield 0.078 g, 80%. Anal. Calcd for $C_{27}H_{43}LaN_6O_8$: C, 45.13; H, 6.03; N, 11.70. Found: C, 45.02; H, 5.89; N, 11.57. HS-MS (ESI$^-$): m/z 616.0924; calcd for $[C_{21}H_{27}LaN_5O_8]^-$ 616.0928. IR (ATR, cm^{-1}): ν 1582 (C═O).

(Et_3NH)[Eu(do3a-pic)]. Yield 0.071 g, 71%. Anal. Calcd for $C_{27}H_{43}EuN_6O_8$: C, 44.32; H, 5.92; N, 11.49. Found: C, 44.53; H, 6.13; N, 11.72. HS-MS (ESI$^-$): m/z 630.1054; calcd for $[C_{21}H_{27}EuN_5O_8]^-$ 630.1077. IR (ATR, cm^{-1}): ν 1596 (C═O).

(Et_3NH)[Gd(do3a-pic)]. Yield 0.073 g, 73%. Anal. Calcd for $C_{27}H_{43}GdN_6O_8$: C, 44.01; H, 5.88; N, 11.40. Found: C, 43.94; H, 5.79; N, 11.57. HS-MS (ESI$^-$): m/z 635.1124; calcd for $[C_{21}H_{27}GdN_5O_8]^-$ 635.1106. IR (ATR, cm^{-1}): ν 1595 (C═O).

(Et_3NH)[Tb(do3a-pic)]. Yield 0.075 g, 75%. Anal. Calcd for $C_{27}H_{43}N_6O_8Tb$: C, 43.91; H, 5.87; N, 11.38. Found: C, 43.83; H, 5.65; N, 11.52. HS-MS (ESI$^-$): m/z 636.1093; calcd for $[C_{21}H_{27}N_5O_8Tb]^-$ 636.1118. IR (ATR, cm^{-1}): ν 1595 (C═O).

(Et_3NH)[Yb(do3a-pic)]. Yield 0.084 g, 82%. Anal. Calcd for $C_{27}H_{43}N_6O_8Yb$: C, 43.08; H, 5.76; N, 11.17. Found: C, 43.22; H, 5.94; N, 10.98. HS-MS (ESI$^-$): m/z 651.1257; calcd for $[C_{21}H_{27}N_5O_8Yb]^-$ 651.1253. IR (ATR, cm^{-1}): ν 1596 (C═O).

(Et_3NH)[Lu(do3a-pic)]. Yield 0.077 g, 75%. Anal. Calcd for $C_{27}H_{43}LuN_6O_8$: C, 42.97; H, 5.74; N, 11.14. Found: C, 43.23; H, 5.79; N, 11.03. HS-MS (ESI$^-$): m/z 652.1293; calcd for $[C_{21}H_{27}LuN_5O_8]^-$ 652.1272. IR (ATR, cm^{-1}): ν 1596 (C═O).

General Procedure for Preparation of (Et_3NH)[Ln(do3a-picOMe)] Complex Salts. The same procedure used for the do3a-pic analogues was followed using do3a-picOMe·5HCl·3H_2O (0.100 g, 0.133 mmol), triethylamine (0.136 g, 1.34 mmol), and Ln(OTf)$_3$ (0.134 mmol, Ln = La, Eu, Gd, Tb, Yb, or Lu) in 2-propanol (15 mL).

(Et_3NH)[La(do3a-picOMe)]. Yield 0.078 g, 77%. Anal. Calcd for $C_{28}H_{45}LaN_6O_9$: C, 44.92; H, 6.06; N, 11.23. Found: C, 44.76; H, 5.91; N, 11.45. HS-MS (ESI$^-$): m/z 646.1039; calcd for $[C_{22}H_{29}LaN_5O_9]^-$ 646.1034. IR (ATR, cm^{-1}): ν 1582 (C═O).

(Et_3NH)[Eu(do3a-picOMe)]. Yield 0.076 g, 74%. Anal. Calcd for $C_{28}H_{45}EuN_6O_9$: C, 44.15; H, 5.96; N, 11.03. Found: C, 44.04; H, 5.86; N, 11.24. HS-MS (ESI$^-$): m/z 660.1157; calcd for $[C_{22}H_{29}EuN_5O_9]^-$ 660.1183. IR (ATR, cm^{-1}): ν 1599 (C═O).

(Et_3NH)[Gd(do3a-picOMe)]. Yield 0.072 g, 70%. Anal. Calcd for $C_{28}H_{45}GdN_6O_9$: C, 43.85; H, 5.91; N, 10.96. Found: C, 42.71; H, 5.77; N, 11.07. HS-MS (ESI$^-$): m/z 665.1214; calcd for $[C_{22}H_{29}GdN_5O_9]^-$ 665.1211. IR (ATR, cm^{-1}): ν 1599 (C═O).

(Et_3NH)[Tb(do3a-picOMe)]. Yield 0.079 g, 76%. Anal. Calcd for $C_{28}H_{45}N_6O_9Tb$: C, 43.75; H, 5.90; N, 10.93. Found: C, 43.53; H, 5.69; N, 11.22. HS-MS (ESI$^-$): m/z 666.1235; calcd for $[C_{22}H_{29}N_5O_9Tb]^-$ 666.1224. IR (ATR, cm^{-1}): ν 1600 (C═O).

(Et_3NH)[Yb(do3a-picOMe)]. Yield 0.089 g, 84%. Anal. Calcd for $C_{28}H_{45}N_6O_9Yb$: C, 42.96; H, 5.79; N, 10.74. Found: C, 42.74; H, 5.53; N, 10.96. HS-MS (ESI$^-$): m/z 681.1384; calcd for $[C_{22}H_{29}N_5O_9Yb]^-$ 681.1359. IR (ATR, cm^{-1}): ν 1600 (C═O).

(Et_3NH)[Lu(do3a-picOMe)]. Yield 0.075 g, 71%. Anal. Calcd for $C_{28}H_{45}LuN_6O_9$: C, 42.86; H, 5.78; N, 10.71. Found: C, 42.80; H, 5.77; N, 10.98. HS-MS (ESI$^-$): m/z 682.1404; calcd for $[C_{22}H_{29}LuN_5O_9]^-$ 682.1378. IR (ATR, cm^{-1}): ν 1599 (C═O).

Computational Methods. All calculations were performed employing hybrid DFT with the B3LYP exchange-correlation functional[72,73] and the Gaussian 09 package (Revision A.02).[74] Full geometry optimizations of the $[Ln(do3a\text{-}pic)]^-$ and $[Ln(do3a\text{-}picOMe)]^-$ (Ln = La, Gd, Yb, or Lu) systems were performed in aqueous solution using the effective core potential (ECP) of Dolg et al. and the related [5s4p3d]-GTO valence basis set for the lanthanides[75] and the 6-31G(d) basis set for C, H, N, and O atoms. No symmetry constraints have been imposed during the optimizations. The default values for the integration grid ("fine") and the SCF energy convergence criteria (10^{-6}) were used. The stationary points found on the potential-energy surfaces as a result of the geometry optimizations have been tested to represent energy minima rather than saddle points via frequency analysis. Solvent effects were evaluated using the polarizable continuum model (PCM), in which the solute cavity is built as an envelope of spheres centered on atoms or atomic groups with appropriate radii. In particular, we used the integral equation formalism (IEFPCM) variant as implemented in Gaussian 09.[76] The relative free energies of the SAP and TSAP conformations were calculated in aqueous solution at the B3LYP/6-31G(d) level, including non-potential-energy contributions (zero-point energies and thermal terms) obtained through frequency analysis. The interconversion between the SAP and the TSAP conformations of the $[Ln(do3a\text{-}pic)]^-$ and $[Ln(do3a\text{-}picOMe)]^-$ complexes (Ln = La or Lu) was investigated by means of the synchronous transit-guided quasi-Newton method.[77] The nature of the saddle points and intermediates was characterized by frequency analysis. The free energy barriers include non-potential-energy contributions (that is, zero-point energies and thermal terms) obtained by frequency analysis.

■ ASSOCIATED CONTENT

Supporting Information. Absorption, excitation, and emission spectra of $[Ln(do3a\text{-}picOMe)]^-$ complexes (Ln = Eu or Tb), ^1H NMR spectra of La^{III} and Lu^{III} complexes, DFT-optimized SAP and TSAP isomers of the $[Gd(do3a\text{-}pic)]^-$ complex, absorption spectra for reacting mixtures Eu−$H_x$do3a-pic, ^1H and ^{13}C NMR data, calculated bond distances of the metal coordination environments (B3LYP), PSEQUAD output files used for determination of stability constants, and optimized Cartesian coordinates for $[Ln(do3a\text{-}pic)]^-$ and $[Ln(do3a\text{-}picOMe)]^-$ (Ln = La, Gd, Yb, or Lu). This material is available free of charge via the Internet at http://pubs.acs.org.

■ AUTHOR INFORMATION

Corresponding Author

*E-mail: carlos.platas.iglesias@udc.es.

■ ACKNOWLEDGMENT

M.R.-F., D.E.-G., A.d.B., T.R.-B., and C.P.-I. thank the Ministerio de Educación y Ciencia (MEC) and Fondo Europeo de Desarrollo Regional (FEDER) (CTQ2006-07875/PPQ and CTQ2009-10721)) and Xunta de Galicia (IN845B-2010/063) for financial support. M.R.-F. thanks the Ministerio de Educación y Ciencia (FPU program) for a predoctoral fellowship. B.B. thanks the Algerian Ministry of Higher Education for financial support. G.T., I.T., and E.R. acknowledge the support given by the Hungarian Scientific Research Found (OTKA K84291). The publication is supported by the TÁMOP 4.2.1/B-09/1/KONV-2010-0007 project. The project is co-financed by the European Union and the European Social Fund. We are grateful to Prof. István Fábián and Dr. Gábor Lente (University of Debrecen) for gaining access to the Applied Photophysics SX 17MV stopped-flow apparatus. This research was performed in the framework of the EU COST Action D38 "Metal-Based Systems for Molecular Imaging Applications". The authors are indebted to the Centro de Supercomputación de Galicia for providing the computer facilities.

■ REFERENCES

(1) (a) Caravan, P.; Ellinson, J. J.; McMurry, T. J.; Lauffer, R. B. *Chem. Rev.* **1999**, *99*, 2293–2352.(b) In *The Chemistry of Contrast Agents in Medical Magnetic Resonance Imaging*; Merbach, A. E.; Tóth, É., Eds.; Wiley: New York, 2001. (c) De Leon-Rodriguez, L. M.; Lubag, A. J. M.; Malloy, C. R.; Martinez, G. V.; Gillies, R. J.; Sherry, A. D. *Acc. Chem. Res.* **2009**, *42*, 948–957. (d) Chan, K. W.-Y.; Wong, W.-T. *Coord. Chem. Rev.* **2007**, *251*, 2428–2451. (e) Terreno, E.; Castelli, D. D.; Viale, A.; Aime, S. *Chem. Rev.* **2010**, *110*, 3019–3042.

(2) (a) Liu, S. *Adv. Drug Delivery Rev.* **2008**, *60*, 1347–1370. (b) Roesch, F. *Radiochim. Acta* **2007**, *95*, 303–311. (c) Volkert, W. A.; Hoffman, T. J. *Chem. Rev.* **1999**, *99*, 2269–2292. (d) Tweedle, M. F. *Acc. Chem. Res.* **2009**, *42*, 958–968.

(3) Parker, D.; Dickins, R. S.; Puschmann, H.; Crossland, C.; Howard, J. A. K. *Chem. Rev.* **2002**, *102*, 1977–2010.

(4) (a) Bünzli, J.-C. G. *Chem. Rev.* **2010**, *110*, 2729–2755. (b) Geissler, D.; Charbonnière, L. J.; Ziessel, R. F.; Butlin, N. G.; Löhmannsröben, H.-G.; Hildebrandt, N. *Angew. Chem., Int. Ed.* **2010**, *49*, 1396–1401.

(5) Latva, M.; Takalo, H.; Mukkala, V.-M.; Matachescu, C.; Rodriguez-Ubis, J. C.; Kankare, J. *J. Lumin.* **1997**, *75*, 149–169.

(6) (a) Wang, X.; Jin, T.; Comblin, V.; Lopez-Mut, A.; Merciny, E.; Desreux, J.-F. *Inorg. Chem.* **1992**, *31*, 1095–1099. (b) Toth, E.; Brucher, E.; Lazar, I.; Toth, I. *Inorg. Chem.* **1994**, *33*, 4070–4076.

(7) (a) Kumar, K.; Chang, C. A.; Francesconi, L. C.; Dischino, D. D.; Malley, M. F.; Gougoutas, J. Z.; Tweedle, M. F. *Inorg. Chem.* **1994**, *33*, 3567–3575. (b) Kumar, K.; Chang, C. A.; Tweedle, M. F. *Inorg. Chem.* **1993**, *32*, 587–593. (c) Kumar, K.; Tweedle, M. F. *Inorg. Chem.* **1993**, *32*, 4193–4199.

(8) Chang, C. A.; Francesconi, L. C.; Malley, M. F.; Kumar, K.; Gougoutas, J. Z.; Tweedle, M. F.; Lee, D. W.; Wilson, L. J. *Inorg. Chem.* **1993**, *32*, 3501–3508.

(9) (a) Urbanczyk-Pearson, L. M.; Femia, F. J.; Smith, J.; Parigi, G.; Duimstra, J. A.; Eckermann, A. L.; Luchinat, C.; Meade, T. J. *Inorg. Chem.* **2008**, *47*, 56–68. (b) Carrera, C.; Digilio, G.; Baroni, S.; Burgio, D.; Consol, S.; Fedeli, F.; Longo, D.; Mortillaro, A.; Aime, S. *Dalton Trans.* **2007**, 4980–4987. (c) Duimstra, J. A.; Femia, F. J.; Meade, T. J. *J. Am. Chem. Soc.* **2005**, *127*, 12847–12855.

(10) (a) Que, E. L.; Gianolio, E.; Baker, S. L.; Wong, A. P.; Aime, S.; Chang, C. J. *J. Am. Chem. Soc.* **2009**, *131*, 8527–8536. (b) Lowe, M. P.; Parker, D.; Reany, O.; Aime, S.; Botta, M.; Castellano, G.; Gianolio, E.; Pagliarin, R. *J. Am. Chem. Soc.* **2001**, *123*, 7601–7609. (c) Manus, L. M.; Mastarone, D. J.; Waters, E. A.; Zhang, X.-Q.; Schultz-Sikma, E. A.; MacRenaris, K. W.; Ho, D.; Meade, T. J. *Nano Lett.* **2010**, *10*, 484–489. (d) Gianolio, E.; Napolitano, R.; Fedeli, F.; Arena, F.; Aime, S. *Chem. Commun.* **2009**, 6044–6046. (e) Lacerda, S.; Campello, M. P.; Marques, F.; Gano, L.; Kubicek, V.; Fouskova, P.; Toth, É.; Santos, I. *Dalton Trans.* **2009**, 4509–4518. (f) Regueiro-Figueroa, M.; Djanashvili, K.; Esteban-Gómez, D.; Chauvin, T.; Toth, E.; de Blas, A.; Rodríguez-Blas, T.; Platas-Iglesias, C. *Inorg. Chem.* **2010**, *49*, 4212–4223.

(11) (a) Koullourou, T.; Natrajan, L. S.; Bhavsar, H.; Pope, S. J. A.; Feng, J.; Narvainen, J.; Shaw, R.; Scales, E.; Kauppinen, R.; Kenwright, A. M.; Faulkner, S. *J. Am. Chem. Soc.* **2008**, *130*, 2178–2179.

(12) (a) Chatterton, N.; Bretonniere, Y.; Pecaut, J.; Mazzanti, M. *Angew. Chem., Int. Ed.* **2005**, *44*, 7595–7598. (b) Charbonnière, L.; Weibel, N.; Estournes, C.; Leuvrey, C.; Ziessel, R. *New J. Chem.* **2004**, *28*, 777–781.

(13) (a) Platas-Iglesias, C.; Mato-Iglesias, M.; Djanashvili, K.; Muller, R. N.; Vander Elst, L.; Peters, J. A.; de Blas, A.; Rodríguez-Blas, T. *Chem.—Eur. J.* **2004**, *10*, 3579–3590. (b) Balogh, E.; Mato-Iglesias, M.; Platas-Iglesias, C.; Tóth, É.; Djanashvili, K.; Peters, J. A.; de Blas, A.; Rodríguez-Blas, T. *Inorg. Chem.* **2006**, *45*, 8719–8728. (c) Mato-Iglesias, M.; Balogh, E.; Platas-Iglesias, C.; Tóth, É.; de Blas, A.; Rodríguez-Blas, T. *Dalton Trans.* **2006**, 5404–5415. (d) Nonat, A.; Fries, P. H.; Pecaut, J.; Mazzanti, M. *Chem.—Eur. J.* **2007**, *13*, 8489–8506. (e) Chatterton, N.; Gateau, C.; Mazzanti, M.; Pecaut, J.; Borel, A.; Helm, L.; Merbach, A. E. *Dalton Trans.* **2005**, 1129–1135. (f) Mameri, S.; Charbonnière, L.; Ziessel, R. *Tetrahedron Lett.* **2007**, *48*, 9132–9136.

(14) (a) Mato-Iglesias, M.; Roca-Sabio, A.; Palinkas, Z.; Esteban-Gómez, D.; Platas-Iglesias, C.; Toth, E.; de Blas, A.; Rodriguez-Blas, T. *Inorg. Chem.* **2008**, *47*, 7840–7851. (b) Nonat, A.; Giraud, M.; Gateau, C.; Fries, P. H.; Helm, L.; Mazzanti, M. *Dalton Trans.* **2009**, 8033–8046. (c) Palinkas, Z.; Roca-Sabio, A.; Mato-Iglesias, M.; Esteban-Gomez, D.; Platas-Iglesias, C.; de Blas, A.; Rodriguez-Blas, T.; Toth, E. *Inorg. Chem.* **2009**, *48*, 8878–8889.

(15) (a) Platas-Iglesias, C.; Piguet, C.; Andre, N.; Bunzli, J.-C. G. *J. Chem. Soc., Dalton Trans.* **2001**, 3084–3091. (b) DÁleo, A.; Piccot, A.; Baldeck, P. L.; Andraud, C.; Maury, O. *Inorg. Chem.* **2008**, *47*, 10269–10279. (c) Chauvin, A.-S.; Gras, S.; Bünzli, J.-C. G. *Org. Biomol. Chem.* **2003**, *1*, 737–740. (d) Tripier, R.; Hollenstein, M.; Elhabiri, M.; Chauvin, A.-S.; Zucchi, G.; Piguet, C.; Bunzli, J.-C. G. *Helv. Chim. Acta* **2002**, *85*, 1915–1929. (e) Piccot, A.; DÁleo, A.; Baldeck, P. L.; Grichine, A.; Duperray, A.; Andraud, C.; Maury, O. *J. Am. Chem. Soc.* **2008**, *130*, 1532–1533.

(16) (a) Teyssot, M.-L.; Nauton, L.; Canet, J.-L.; Cisnetti, F.; Chevry, A.; Gautier, A. *Eur. J. Org. Chem.* **2010**, 3507–3515. (b) Chamas, Z. E. A.; Guo, X.; Canet, J.-L.; Gautier, A.; Boyer, D.; Mahiou, R. *Dalton Trans.* **2010**, *39*, 7091–7097.

(17) Zech, S. G.; Sun, W.-C.; Jacques, V.; Caravan, P.; Astashkin, A. V.; Raitsimring, A. M. *ChemPhysChem* **2005**, *6*, 2570–22577.

(18) D'Aléo, A.; Allali, M.; Picot, A.; Baldeck, P. L.; Toupet, L.; Andraud, C.; Maury, O. *C. R. Chimie* **2010**, *13*, 681–690.

(19) Kaspersen, F. M.; Reinhoudt, D. N.; Verboom, W.; Van Staveren, C. J. PCT Int. Appl. WO 9501346 A1 19950112, 1995.

(20) McKenzie, B. M.; Miller, A. K.; Wojtecki, R. J.; Johnson, J. C.; Burke, K. A.; Tzeng, K. A.; Mather, P. T.; Rowan, S. J. *Tetrahedron* **2008**, *64*, 8488–8495.

(21) Barge, A.; Tei, L.; Upadhyaya, D.; Fedeli, F.; Beltrami, L.; Stefania, R.; Aime, S.; Cravotto, G. *Org. Biomol. Chem.* **2008**, *6*, 1176–1184.

(22) Chaves, S.; Delgado, R.; Dasilva, J. J. R. F. *Talanta* **1992**, *39*, 249–254.

(23) Burai, L.; Fabian, I.; Kiraly, R.; Szilagyi, E.; Brucher, E. *J. Chem. Soc., Dalton Trans.* **1998**, 243–248.

(24) Cacheris, W. P.; Nickle, S. K.; Sherry, A. D. *Inorg. Chem.* **1987**, *26*, 958–960.

(25) Amorim, M. T. S.; Delgado, R.; Dasilva, J. J. R. *Polyhedron* **1992**, *11*, 1891–1899.

(26) Wu, S. L.; Horrocks, W. D. *Anal. Chem.* **1996**, *68*, 394–401.

(27) Bianchi, A.; Calabi, L.; Giorgi, C.; Losi, P.; Mariani, P.; Paoli, P.; Rossi, P.; Valtancoli, B.; Virtuani, M. *J. Chem. Soc., Dalton Trans.* **2000**, 697–705.

(28) Ferreirós-Martínez, R.; Esteban-Gómez, D.; Platas-Iglesias, C.; de Blas, A.; Rodríguez-Blas, T. *Dalton Trans.* **2008**, 5754–5765.
(29) Roca-Sabio, A.; Mato-Iglesias, M.; Esteban-Gomez, D.; de Blas, A.; Rodriguez-Blas, T.; Platas-Iglesias, C. *Dalton Trans.* **2011**, *40*, 384–392.
(30) Roca-Sabio, A.; Mato-Iglesias, M.; Esteban-Gomez, D.; Toth, E.; de Blas, A.; Platas-Iglesias, C.; Rodriguez-Blas, T. *J. Am. Chem. Soc.* **2009**, *131*, 3331–3341.
(31) Martell, A. E.; Smith, R. M.; Motekaitis, R. J. *Critically Selected Stability Constants of Metal Complexes*, Database Version 8.0, 2004.
(32) (a) Chatterton, N.; Bretonnière, Y.; Pécaut, J.; Mazzanti, M. *Angew. Chem., Int. Ed.* **2005**, *117*, 7595–7598. (b) Bretonnière, Y.; Mazzanti, M.; Pécaut, J.; Dunand, F.; Merbach, A. E. *Inorg. Chem.* **2001**, *40*, 6737–6745. (c) Weibel, N.; Charbonnière, L.; Ziessel, R. *Tetrahedron Lett.* **2006**, 1793–1796.
(33) Bünzli, J.-C. G.; Piguet, C. *Chem. Soc. Rev.* **2005**, *34*, 1048–1077.
(34) (a) Weissmann, S. I. *J. Chem. Phys.* **1942**, *10*, 214–217. (b) Sabbatini, N.; Guardigli, M.; Lehn, J.-M. *Coord. Chem. Rev.* **1993**, *123*, 201–228.
(35) (a) Supkowski, R. M.; Horrocks, W. D. W., Jr. *Inorg. Chim. Acta* **2002**, *340*, 44–48. (b) Horrocks, W. D. W., Jr.; Sudnick, D. R. *J. Am. Chem. Soc.* **1979**, *101*, 334–340. (c) Beeby, A.; Clarkson, I. M.; Dickins, R. S.; Faulkner, S.; Parker, D.; Royle, L.; de Sousa, A. S.; Williams, J. A. G.; Woods, M. *J. Chem. Soc., Perkin Trans. 2* **1999**, 493–503. (d) Stein, G.; Würzberg, E. *J. Chem. Phys.* **1975**, *62*, 208–213. (e) Kimura, T.; Kato, Y. *J. Alloys Compd.* **1998**, *275*, 806–810.
(36) Quici, S.; Marzanni, G.; Cavazzini, M.; Anelli, P. L.; Botta, M.; Gianolio, E.; Accorsi, G.; Armaroli, N.; Barigelletti, F. *Inorg. Chem.* **2002**, *41*, 2777–2784.
(37) (a) Werts, M. H. V.; Jukes, R. T. F.; Verhoeven, J. W. *Phys. Chem. Chem. Phys.* **2002**, *4*, 1542–1548. (b) Kadjane, P.; Charbonnière, L.; Camerel, F.; Lainé, P. P.; Ziessel, R. *J. Fluoresc.* **2008**, *18*, 119–129.
(38) Tripier, R.; Platas-Iglesias, C.; Boos, A.; Morfin, J.-F.; Charbonnière, L. *Eur. J. Inorg. Chem.* **2010**, 2735–2745.
(39) Gassner, A.-L.; Duhot, C.; Bünzli, J.-C. G.; Chauvin, A.-S. *Inorg. Chem.* **2008**, *47*, 7802–7812.
(40) McConnell, H. M. *J. Chem. Phys.* **1957**, *27*, 226–229.
(41) Aime, S.; Botta, M.; Ermondi, G. *Inorg. Chem.* **1992**, *31*, 4291–4299.
(42) (a) Karplus, M. *J. Am. Chem. Soc.* **1963**, *85*, 2870–2871. (b) Geraldes, C. F. G. C.; Sherry, A. D.; Kiefer, G. E. *J. Magn. Reson.* **1992**, *97*, 290–304.
(43) (a) Corey, E. J.; Bailar, J. C., Jr. *J. Am. Chem. Soc.* **1959**, *81*, 2620–2629. (b) Beattie, J. K. *Acc. Chem. Res.* **1971**, *4*, 253–259.
(44) (a) Aime, S.; Botta, M.; Fasano, M.; Marques, M. P. M.; Geraldes, C. F. G. C.; Pubanz, D.; Merbach, A. E. *Inorg. Chem.* **1997**, *36*, 2059–2068. (b) Hoeft, S.; Roth, K. *Chem. Ber.* **1993**, *126*, 869–873.
(45) Seitz, M.; Oliver, A. G.; Raymond, K. N. *J. Am. Chem. Soc.* **2007**, *129*, 11153–11160.
(46) (a) Aime, S.; Barge, A.; Benetollo, F.; Bombieri, G.; Botta, M.; Fulvio, U. *Inorg. Chem.* **1997**, *36*, 4287–4289. (b) Aime, S.; Barge, A.; Botta, M.; Fasano, M.; Ayala, J. D.; Bombieri, G. *Inorg. Chim. Acta* **1996**, *246*, 423–429.
(47) Piguet, C.; Bünzli, J.-C. G.; Bernardinelli, G.; Bochet, C. G.; Froidevaux, P. *J. Chem. Soc., Dalton Trans.* **1995**, 83–97.
(48) Cosentino, U.; Villa, A.; Pitea, D.; Moro, G.; Barone, V.; Maiocchi, A. *J. Am. Chem. Soc.* **2002**, *124*, 4901–4909.
(49) Peters, J. A.; Huskens, J.; Raber, D. J. *Prog. NMR Spectrosc.* **1996**, *28*, 283–350.
(50) Di Bari, L.; Pescitelli, G.; Sherry, A. D.; Woods, M. *Inorg. Chem.* **2005**, *44*, 8391–8398.
(51) Forsberg, J. H.; Delaney, R. M.; Zhao, Q.; Harakas, G.; Chandran, R. *Inorg. Chem.* **1995**, *34*, 3705–3715.
(52) Rudovsky, J.; Cigler, P.; Kotek, J.; Hermann, P.; Vojtisek, P.; Lukes, I.; Peters, J. A.; Vander Elst, L.; Muller, R. N. *Chem.—Eur. J.* **2005**, *11*, 2373–2384.
(53) Jacques, V.; Desreux, J. F. *Inorg. Chem.* **1994**, *33*, 4048–4053.
(54) (a) Purgel, M.; Baranyai, Z.; de Blas, A.; Rodríguez-Blas, T.; Bányai, I.; Platas-Iglesias, C.; Tóth, I. *Inorg. Chem.* **2010**, *49*, 4370–4382. (b) Regueiro-Figueroa, M.; Esteban-Gómez, D.; de Blas, A.; Rodríguez-Blas, T.; Platas-Iglesias, C. *Eur. J. Inorg. Chem.* **2010**, 3586–3595.
(55) Di Vaira, M.; Stoppioni, P. *New J. Chem.* **2002**, *26*, 136–144.
(56) Natrajan, L. S.; Khoabane, N. M.; Dadds, B. L.; Muryn, C. A.; Pritchard, R. G.; Heath, S. L.; Kenwright, A. M.; Kuprov, I.; Faulkner, S. *Inorg. Chem.* **2010**, *49*, 7700–7709.
(57) Brucher, E.; Sherry, A. D. *Inorg. Chem.* **1990**, *29*, 1555–1559.
(58) Balogh, E.; Tripier, R.; Ruloff, R.; Toth, E. *Dalton Trans.* **2005**, 1058–1065.
(59) Moreau, J.; Guillon, E.; Pierrard, J.-C.; Rimbault, J.; Port, M.; Aplincourt, M. *Chem.—Eur. J.* **2004**, *10*, 5218–5232.
(60) Tircso, G.; Kovacs, Z.; Sherry, A. D. *Inorg. Chem.* **2006**, *45*, 9269–9280.
(61) Szilagyi, E.; Toth, E.; Kovacs, Z.; Platzek, J.; Raduchel, B.; Brucher, E. *Inorg. Chim. Acta* **2000**, *298*, 226–234.
(62) Balogh, E.; Tripier, R.; Fouskova, P.; Reviriego, F.; Handel, H.; Toth, E. *Dalton Trans.* **2007**, 3572–3581.
(63) Sarka, L.; Burai, L.; Brucher, E. *Chem.—Eur. J.* **2000**, *6*, 719–724.
(64) Brucher, E.; Laurenczy, G.; Makra, Z. *Inorg. Chim. Acta* **1987**, *139*, 141–142.
(65) Kumar, K.; Tweedle, M. F. *Pure Appl. Chem.* **1993**, *65*, 515–520.
(66) Wedeking, P.; Kumar, K.; Tweedle, M. F. *Magn. Reson. Imaging* **1992**, *10*, 641–648.
(67) Haas, Y.; Stein, G. *J. Phys. Chem.* **1971**, *75*, 3668–3677.
(68) Nakamaru, K. *Bull. Chem. Soc. Jpn.* **1982**, *55*, 2697–2705.
(69) Olmsted, J. *J. Phys. Chem.* **1979**, *83*, 2581–2584.
(70) Irving, H. M.; Miles, M. G.; Pettit, L. D. *Anal. Chim. Acta* **1967**, *38*, 475–488.
(71) Zekany, L.; Nagypal, I. In *Computational Methods for the Determination of Formation Constants*; Leggett, D. J., Ed.; Plenum Press: New York, 1985; p 291.
(72) Becke, A. D. *J. Chem. Phys.* **1993**, *98*, 5648–5652.
(73) Lee, C.; Yang, W.; Parr, R. G. *Phys. Rev. B* **1988**, *37*, 785–789.
(74) Frisch, M. J.; Trucks, G. W.; Schlegel, H. B.; Scuseria, G. E.; Robb, M. A.; Cheeseman, J. R.; Scalmani, G.; Barone, V.; Mennucci, B.; Petersson, G. A.; Nakatsuji, H.; Caricato, M.; Li, X.; Hratchian, H. P.; Izmaylov, A. F.; Bloino, J.; Zheng, G.; Sonnenberg, J. L.; Hada, M.; Ehara, M.; Toyota, K.; Fukuda, R.; Hasegawa, J.; Ishida, M.; Nakajima, T.; Honda, Y.; Kitao, O.; Nakai, H.; Vreven, T.; Montgomery, Jr., J. A.; Peralta, J. E.; Ogliaro, F.; Bearpark, M.; Heyd, J. J.; Brothers, E.; Kudin, K. N.; Staroverov, V. N.; Kobayashi, R.; Normand, J.; Raghavachari, K.; Rendell, A.; Burant, J. C.; Iyengar, S. S.; Tomasi, J.; Cossi, M.; Rega, N.; Millam, N. J.; Klene, M.; Knox, J. E.; Cross, J. B.; Bakken, V.; Adamo, C.; Jaramillo, J.; Gomperts, R.; Stratmann, R. E.; Yazyev, O.; Austin, A. J.; Cammi, R.; Pomelli, C.; Ochterski, J. W.; Martin, R. L.; Morokuma, K.; Zakrzewski, V. G.; Voth, G. A.; Salvador, P.; Dannenberg, J. J.; Dapprich, S.; Daniels, A. D.; Farkas, Ö.; Foresman, J. B.; Ortiz, J. V.; Cioslowski, J.; Fox, D. J. *Gaussian 09*, Revision A.01; Gaussian, Inc., Wallingford, CT, 2009.
(75) Dolg, M.; Stoll, H.; Savin, A.; Preuss, H. *Theor. Chim. Acta* **1989**, *75*, 173–194.
(76) Tomasi, J.; Mennucci, B.; Cammi, R. *Chem. Rev.* **2005**, *105*, 2999–3093.
(77) (a) Peng, C.; Ayala, P. Y.; Schlegel, H. B.; Frisch, M. J. *J. Comput. Chem.* **1996**, *17*, 49–56. (b) Peng, C.; Schlegel, H. B. *Isr. J. Chem.* **1994**, *33*, 449–454.